JOURNAL OF GEOPHYSICAL RESEARCH, VOL. 105, NO. D8, PAGES 9741-9765, APRIL 27, 2000

Sensitivity of sulphate aerosol size distributions and CCN concentrations over North America to SO_x emissions and H_2O_2 concentrations

K. von Salzen,[1,2] H. G. Leighton,[1] P. A. Ariya,[1] L. A. Barrie,[3,4] S. L. Gong,[3] J.-P. Blanchet,[5] L. Spacek,[5] U. Lohmann,[6] and L. I. Kleinman[7]

Abstract. To assess the influence of aerosols on climate, the Northern Aerosol Regional Climate Model (NARCM) is currently being developed. NARCM includes size-segregated aerosols as prognostic and interactive constituents. In this paper, the model is being applied to sulphate aerosol over North America during time periods in July and December 1994. The results give evidence for considerable regional and seasonal variations in sulphate aerosol size distributions over North America. Comparisons of the results with different observations yield a reasonably good agreement in terms of meteorological and physicochemical parameters. Some of the differences in sulphate concentrations and wet deposition rates can be attributed to differences in cloud amounts and precipitation between model results and observations. Indirect tests of the simulated aerosol mass mean diameters are also encouraging. Additional simulations for hypothetical decreases in anthropogenic sulphur emissions and increases in hydrogen peroxide (H_2O_2) background concentrations are performed for the same time periods to study the responses of concentration, size distribution, and wet deposition of sulphate aerosol to these changes. Also, responses of cloud condensation nuclei (CCN) number concentrations are investigated. The simulation results show that sulphate aerosol concentrations respond almost linearly in both time periods to decreases in sulphur emissions but that CCN number concentrations respond nonlinearly due to decreases in sulphate mass mean diameters. Especially for the December period, increases in hydrogen peroxide background concentrations lead to increases in CCN number concentrations at critical diameters larger than about 0.07 μm. These results lead to the hypothesis that increased in-cloud oxidation in convective clouds due to future increases in oxidant concentrations may produce larger CCN which eventually can be easily activated in subsequently forming stratiform clouds.

[1]Department of Atmospheric and Oceanic Sciences, McGill University, Montreal, Quebec, Canada.

[2]Now at Canadian Centre for Climate Modelling and Analysis, University of Victoria, Victoria, British Columbia, Canada.

[3]Meteorological Service of Canada, Toronto, Ontario, Canada.

[4]Now at Environmental Molecular Science Laboratory, Pacific Northwest National Laboratory, Richland, Washington.

[5]Earth Sciences Department, University of Quebec at Montreal, Montreal, Quebec, Canada.

[6]Department of Physics, Dalhousie University, Halifax, Nova Scotia, Canada.

[7]Environmental Chemistry Division, Brookhaven National Laboratory, Upton, New York.

Paper number 2000JD900027.
0148-0227/00/2000JD900027$09.00

1. Introduction

The present radiative forcing by anthropogenic sulphate aerosol particles represents a perturbation to climate with a magnitude possibly of the order of the forcing due to the greenhouse gas accumulation since preindustrial times, but of opposite sign [*Charlson et al.*, 1992; *Houghton et al.*, 1996]. Although there is widespread acknowledgement of the importance of sulphate aerosols in radiative forcing of climate and of the effects of acidic deposition on the environment, relatively little is known about the response of these effects to changing sulphur oxide (SO_x) emissions and oxidant concentrations.

Whereas emissions of sulphur oxides from North America have decreased by about 15% from 1970 to the beginning of the 1990s after several decades of considerable increase [*Shannon*, 1992; *Graedel et al.*, 1995], other regions are still experiencing increasing emissions

[*Houghton et al.*, 1992]. For example, Asian emissions of SO_2 are expected to grow from 32 Mt in 1990 to more than 110 Mt in 2020 if no control measures are taken [*Foell et al.*, 1995]. The aerosol sulphate concentrations and deposition fluxes do not necessarily vary in proportion to the SO_2 emissions. *Holland et al.* [1999] showed that the median SO_4^{2-} concentrations over the eastern United States have declined by 26% between 1989 and 1995, which is smaller than the corresponding decline in median SO_2 concentrations (35%). At various United States National Parks in the northwest and east, *Eldred and Cahill* [1994] observed mean annual increases in particulate SO_4^{2-} concentrations of up to about 3% from 1982 to 1992 although sulphur emissions have not increased in these regions during that period.

Nonlinear responses of SO_4^{2-} concentrations to sulphur oxide emissions may be caused by disproportional changes in in-cloud production of sulphate aerosol. Estimated contributions of in-cloud oxidation of SO_2 to total sulphate production are about 80 to 90% on the global scale [*Lelieveld and Heintzenberg*, 1992] and about 40 to 70% over the northeastern United States [*Scott*, 1982]. In contrast to a linear relationship between the gas phase SO_4^{2-} production and SO_2 concentrations [*Stockwell and Calvert*, 1983; *Meagher et al.*, 1984], the response of SO_4^{2-} in-cloud production may be less than proportional to reductions of sulphur dioxide concentrations. Upon aqueous phase conversion of SO_2 to SO_4^{2-}, the most reactive oxidant (usually hydrogen peroxide) can become depleted. Thus the SO_4^{2-} production may be oxidant-limited, and unreacted SO_2 cannot cause further production of SO_4^{2-} as long as oxidants remain depleted. Consequently, reductions of sulphur oxide emissions may not cause equivalent reductions in SO_4^{2-} production and SO_4^{2-} wet deposition. *Clark et al.* [1987] and *Meagher et al.* [1990] found that oxidant limitation effects may be very important and in-cloud sulphate production over eastern North America is mainly nonlinear. Results of the Regional Acid Deposition Model (RADM) showed that for a 50% decrease in sulphur emissions some regions in eastern North America may exhibit reductions of annual wet sulphur deposition of only up to 38%, depending on the regional sulphur emissions [*Dennis et al.*, 1991].

Another, less well recognized, cause for the observed nonlinear responses of sulphate to past changes in SO_x emissions is an increased photochemical production of oxidants due to global and regional increases in CH_4, CO, and NO emissions. For example, ice core samples drilled at Summit Greenland give evidence for a 60% increase in hydrogen peroxide (H_2O_2) concentrations during the last 150 years [*Anklin and Bales*, 1997]. *Thompson et al.* [1989] pointed out that H_2O_2 increases from 1980 to 2030 could be 100% or more in the urban boundary layer.

Whereas the effects of changing SO_x emissions on in-cloud production and wet deposition of SO_4^{2-} have been intensely discussed in the 1980s, the responses in terms of SO_4^{2-} concentrations and aerosol sizes to changing SO_x emissions and oxidant concentrations are not well understood. The sizes of the aerosol particles have a strong effect on the total radiation balance, since the aerosol optical depth and the activation of aerosol particles to cloud droplets are sensitive to the aerosol size [e.g., *Albrecht*, 1989; *Lelieveld and Heintzenberg*, 1992; *Tang*, 1997]. *Choularton et al.* [1998] concluded from observations in a hill cap cloud that chemical processing of CCN activated by large updrafts in hill cap clouds and in convective clouds makes these CCN available for activation in stratocumulus clouds.

To assess the influence of aerosols on climate, the Northern Aerosol Regional Climate Model (NARCM) is being developed. NARCM includes size-segregated aerosols as prognostic and interactive constituents. This paper describes the NARCM parameterizations of aerosol sulphate production by clear-sky homogeneous nucleation and sulphuric acid (H_2SO_4) condensation on preexisting aerosol, and by in-cloud oxidation of SO_2. The model has been applied over eastern North America since the relatively high SO_4^{2-} concentrations in this region have a potentially strong effect on the radiation balance. According to *Malm et al.* [1994], about two thirds of the extinction over the eastern United States can be attributed to sulphate aerosol.

To validate the model, results of 2-week periods in summer and winter 1994 are being compared with observations. For the same periods, simulations of the effects of changing anthropogenic sulphur emissions and H_2O_2 concentrations on sulphate aerosol were performed with artificial reductions in anthropogenic SO_x emissions and increases in H_2O_2 concentrations. The results are discussed with respect to sulphate aerosol concentrations, size distribution, and wet deposition. The importance of changes in atmospheric chemistry on cloud condensation nuclei (CCN) number concentrations are also discussed.

2. Northern Aerosol Regional Climate Model (NARCM)

NARCM is a limited-area model which links existing and well established climate model approaches with a comprehensive treatment of aerosols. Simulated aerosol size distributions are used in on-line calculations of aerosol optical depth and extinction.

The dynamical kernel of NARCM is identical to the Canadian Regional Climate Model (CRCM) [*Laprise et al.*, 1997; *Caya and Laprise*, 1999]. The model equations are solved in a fully elastic and nonhydrostatic mode. For advection of water vapor and tracers, the semi-Lagrangian method is used [*Caya et al.*, 1995]. In this paper, the chemical processes are calculated on a polar-stereographic grid by use of 46 longitude and 36 latitude grid points for a given a horizontal grid spacing of 145 km at 60°N. The vertical grid is discretised using terrain-following Gal-Chen coordinates and 22 grid

points between the surface and the top level at 14 hPa. The time step of NARCM is 20 min.

The parameterizations of radiation, turbulent diffusion, surface processes, and convective clouds in NARCM are taken from the General Circulation Model of the Canadian Centre for Climate Modelling and Analysis [*McFarlane et al.,* 1992; *Verseghy et al.,* 1993; *Zhang and McFarlane,* 1995]. Vertical fluxes of momentum, heat, and moisture due to turbulent processes are represented using a mixing-length formulation in the free atmosphere, while those at the surface are calculated from similarity theory.

Cumulus clouds are represented in NARCM by a bulk model including the effects of entrainment and detrainment on the updraft and downdraft convective mass fluxes [*Zhang and McFarlane,* 1995]. An adjustment closure for reversible ascents of undiluted air parcels from subcloud layers based on the convective available potential energy (CAPE) is used. Although only deep convection is considered in the parameterization, the scheme is also applied to shallow convection. Organized entrainment is assumed to depend on buoyancy, and detrainment occurs at cloud top.

Stratiform clouds are included in NARCM by a parameterization based on *Lohmann and Roeckner* [1996]. Its main characteristic is the separate treatment of cloud water and cloud ice as prognostic variables. In this scheme the bulk microphysics parameterizations for warm phase processes are adapted from parameterizations of the stochastic collection equation [*Beheng,* 1994], while the parameterizations of the mixed and ice phases were developed originally for a mesoscale model [*Levkov et al.,* 1992]. Parameterized microphysical processes are condensational growth of cloud droplets, depositional growth of ice crystals, homogeneous, heterogeneous and contact freezing of cloud droplets, autoconversion of cloud droplets, aggregation of ice crystals, accretion of cloud ice and cloud droplets by snow, of cloud droplets by rain, evaporation of cloud water and rain, sublimation of cloud ice and snow, and melting of cloud ice and snow. The number of cloud droplets, which is a parameter in the autoconversion rate of cloud droplets, is empirically related to the sulphate aerosol mass in the current version of NARCM [*Boucher and Lohmann,* 1995]. In future versions, cloud droplet concentrations will be linked to the aerosol size distribution.

In the model, SO_2 is mainly emitted from industrial sources on the continents. A small fraction of the SO_2 may also be produced by gas-phase reactions of hydrogen sulfide (H_2S) and dimethylsulfide (DMS) from natural sources with the hydroxyl radical (OH) and the nitrate radical (NO_3) (L. Spacek et al., NARCM aerosol model applied to eastern North America LITE shuttle measurement period, submitted to *Journal of Geophysical Research,* 1999, hereinafter referred to as Spacek et al., submitted manuscript, 1999). Details on the treatment of the emissions of these species are given in section 3.1.

Aerosol species included in the model version used in this study are sulphate and seasalt. For each species, size distributions with 12 bins (or sections) are used for the dry aerosol (at 0% relative humidity), with sizes ranging from $D_p = 0.01$ μm to $D_p = 41$ μm. Aerosol processes considered are homogeneous nucleation, coagulation, in-cloud production, condensation of water vapor and H_2SO_4 on preexisting aerosol, gravitational settling, and deposition. These processes, as well as diffusion, advection, and emissions, are calculated on-line at each model time step. For all chemical and microphysical processes, an internally mixed aerosol for sulphate and seasalt is assumed in each bin.

In the following sections, different model attributes of great importance to this study, such as in-cloud production of aerosol, gas-to-particle conversion, emissions, and deposition, are described. For details on the treatment of gas-phase processes, coagulation, meteorological processes, and additional model tests, the reader is referred to Spacek et al. (submitted manuscript, 1999).

2.1. In-Cloud Production of Sulphate

In NARCM the in-cloud oxidation of S(IV) (= SO_2, HSO_3^-, SO_3^{2-}) is parameterized differently for convective and stratiform clouds. For both cloud types in the model, oxidation occurs with respect to hydrogen peroxide and ozone (O_3) as oxidants. The availability of sulphur dioxide and hydrogen peroxide and the impact of ammonia, nitric acid and carbon dioxide on the in-cloud oxidation rates are explicitly included in the parameterizations. To increase the model efficiency, a bulk phase approach has been used instead of a more accurate but potentially expensive size-dependent approach to cloud chemistry.

Within the cloudy part of a grid box, the first-order rate constant (in s^{-1}) of S(IV) oxidation is given by the following expression:

$$F = \left| \frac{1}{C_{S(IV)}} \frac{dC_{S(IV)}}{dt} \right| = F_1 C_{O_3} + F_2 C_{H_2O_2} , \quad (1)$$

where $C_{S(IV)}$ is the total concentration of S(IV) (gas phase plus dissolved), C_{O_3} is the total concentration of ozone, and $C_{H_2O_2}$ is the total concentration of hydrogen peroxide. The effective rate constants F_1 and F_2 in (1) are given in Appendix A.

To take into account the dependence of the oxidation rates on the pH, the H^+ concentration is calculated from the ion balance

$$[H^+] + [NH_4^+] = [OH^-] + 2[SO_4^{2-}] + 2[SO_3^{2-}] + [HSO_3^-] + [NO_3^-] + [HCO_3^-] , \quad (2)$$

which is efficiently solved by an iterative calculation using an adapted version of the approach of *Tremblay and Leighton* [1986]. The effects of seasalt and crustal aerosol on the pH are currently not included in NARCM but will be included in future model versions.

Since (1) has been derived for bulk phase concentrations but NARCM simulates size-segregated sulphate aerosol, a simple approach has been developed to distribute additional SO_4^{2-} produced by in-cloud oxidation over the bins of the activated aerosol. In NARCM the production of SO_4^{2-} within individual cloud droplets of different size is approximated as a purely volume controlled process. It is assumed that the cloud droplets have identical chemical compositions and transport limitation effects can be neglected for the gas and aqueous chemical species. In order to conserve total droplet and aerosol number concentrations it is necessary to consider the growth of the activated sulphate aerosol by in-cloud production of SO_4^{2-}. Using these assumptions, the rate constant F_i for bin i can be approximated as function of the bulk rate constant F (see Appendix B):

$$F_i = F\left(x_i + \frac{x_{i-1}}{3\,\Delta\varphi_{i-1}\,\ln 10} - \frac{x_i}{3\,\Delta\varphi_i\,\ln 10}\right), \quad (3)$$

with the fractional SO_4^{2-} concentration $x_i = C_i/\sum_j C_j$ in activated bin i. In (3), $\Delta\varphi_i$ is the width of bin i, with the dimensionless aerosol size given by $\varphi = \log(D_p^{\rm dry}/D_p^0)$, where $D_p^{\rm dry}$ is the dry particle diameter (in μm) and $D_p^0 = 1$ μm is a reference diameter.

The parameterization of the aerosol activation is described by Spacek et al. (submitted manuscript, 1999). It is based on an empirical relationship between observed cloud droplet number concentrations (CDNC) and aerosol number concentrations [*Martin et al.*, 1994]. In the cloudy parts of the grid boxes, the critical aerosol diameter is calculated from the total dry aerosol size distribution in the grid box, using the assumption that the concentration of activated aerosol particles is equal to the concentration of cloud droplets given by the empirical relationship.

Several studies have shown that the simplifying assumption of bulk chemical cloud drop composition may not be well justified for real clouds in which the pH may vary as a function of droplet size [e.g., *Roelofs*, 1992; *Gurciullo and Pandis*, 1997]. *Collett et al.* [1994] showed that about one third of cloud water samples collected from several sites throughout the United States are believed to have experienced more than 20% enhancement in in-cloud oxidation rates compared to what would have been expected for bulk composition. They found that errors due to a bulk approach are high for low oxidant concentrations which is, for example, the case in winter. On this basis, NARCM may tend to underpredict the in-cloud production of sulphate aerosol.

2.1.1. Stratiform clouds. The parameterization of oxidation in subgrid-scale stratiform clouds uses the common operator splitting technique for transport processes and chemical reactions during the model time step. Tendencies of S(IV) and SO_4^{2-} are calculated for given cloud water mixing ratios and fractional cloudiness by using the cloud microphysics scheme of *Lohmann and Roeckner* [1996]. Concentrations $C_s^{t+\Delta t}$ within the cloudy parts of the grid cells at the time $t + \Delta t$ are calculated by applying the Euler Backward Iterative (EBI) method [e.g., *Hertel et al.*, 1993] which may be written for S(IV) as

$$C_s^{t+\Delta t} = C_s^t - \Delta t\, F^{t+\Delta t}\, C_s^{t+\Delta t}, \quad (4)$$

with the internal chemistry time step Δt and the first-order rate constant $F^{t+\Delta t}$ given by (1). C_s^t is initialized with the grid cell averaged S(IV) concentrations at the beginning of each model time step. Owing to the high accuracy of the EBI method, efficient calculations using only two subdivisions of the model time step are achieved.

Sulphate produced in the clouds may eventually be removed by formation of precipitation. At each time step, it is assumed that the fraction of activated sulphate aerosol removed by this process is equal to the fraction of condensed water converted into precipitation in the cloudy parts of the grid boxes. Below the cloud, scavenging of aerosol by rain is parameterized according to the approach of *Slinn* [1984].

2.1.2. Convective clouds. The formation of SO_4^{2-} in convective clouds may be strongly limited by the available amounts of S(IV) and oxidants due to insufficient entrainment and high reaction rates within convective clouds [e.g., *Meagher et al.*, 1990; *Laj et al.*, 1997]. The effects of entrainment and detrainment on the balances of water vapor and energy of convective clouds have been studied extensively and the effects have been parameterized for subgrid-scale cumulus ensembles, but no corresponding parameterization for reacting chemical species existed until recently.

Our parameterization of sulphur transport and chemistry in convective clouds is based on a simplified version of the plume ensemble concept proposed by *Arakawa and Schubert* [1974]. Corresponding to the parameterization of water vapor transport by *Zhang and McFarlane* [1995], the effects of convective transport and chemical reactions on grid cell averaged concentrations C of reacting chemical species (in molecules per kg air) are calculated in our parameterization from:

$$\frac{\partial C}{\partial t} = \frac{1}{\rho}\left[(M_u + M_d)\,\frac{\partial C}{\partial z} + D_u\,(C_u - C)\right], \quad (5)$$

where M_u is the upward mass flux of the air within the convective region, M_d is the respective downward mass flux, D_u is the detrainment rate, and ρ is the air density [*Lohmann et al.*, 1999].

The updraft concentration C_u of each reacting species in (5) is calculated from a quasi steady state mass balance within the updraft region. For example, the mass balance of S(IV) has the form

$$\frac{\partial M_u C_u}{\partial z} = E_u C - D_u C_u - C_0 M_u f_0 C_u - \rho\, b\, F\, C_u, \quad (6)$$

where E_u is the entrainment rate.

The third term on the right-hand side in (6) represents transfer of the species from cloud to rain droplets

according to *Feichter et al.* [1996]. C_0 accounts for conversion of cloud water into rain water [*Lord,* 1982]. The fraction f_0 of S(IV) dissolved in the cloud droplets is calculated as a function of the pH. For the SO_4^{2-} mass balance it is assumed that the sulphate aerosol for particles with diameters larger than the critical diameter are completely activated ($f_0 = 1$). It should be noted that the scavenging of sulphate by rain below the cumulus clouds corresponds to the approach given for stratiform clouds in section 2.1.1.

The last term in (6) represents the depletion of S(IV) due to in-cloud oxidation, with F given by (1) for the microphysical and chemical parameters of the updrafts. The fractional cloudiness b is calculated by using the approach of *Xu and Krueger* [1991] with a maximum value of $b = 0.25$ for deep convection [*Slingo,* 1987].

For all reactive tracers a discrete version of (6) is solved by forward integration in the vertical direction at given entrainment and detrainment rates between cloud base and cloud top. Due to the nonlinear relationships between the tracers through the oxidation term, up to four iterations are performed at each cloudy grid box. The final solutions of Eq. (6) are subsequently used to calculate the tendencies in Eq. (5) at the cloudy grid points using a semi-implicit method [*Zhang and McFarlane,* 1995].

2.1.3. Simplifications for nonsulphur species. In contrast to the aerosol species, SO_2, DMS, and H_2S, the concentrations of other chemical species are not explicitly calculated in NARCM. Instead, grid cell averaged concentrations of the NO_3^--species (HNO_3+NO_3^-), NH_4^+-species (NH_3+NH_4^+), C-species (CO_2+HCO_3^-), and O_3 are prescribed as three-dimensional parameters at each grid point and time step in NARCM and are used to calculate the pH (equation. (2)) and in-cloud oxidation rates. For sulphate production in convective clouds the updraft concentrations of these species are diagnosed and depend on calculated scavenging, entrainment and detrainment rates (compare with equation (6)). In stratiform clouds the precalculated values are used without taking into account modifications by cloud processes in the simulation. This approach is based on the usual assumption that the effects of entrainment, detrainment, scavenging, and chemical processes are negligible for the concentrations of these species in stratiform clouds; that is, there are no significant sources or sinks for the species in the clouds.

In NARCM the concentrations of the prescribed species are provided with a 1-month time resolution from simulations with two models. The ammonium concentrations are from simulations with a global model of the ammonia cycle [*Dentener and Crutzen,* 1994]. The other species (except C-species) are provided by the global chemical transport model MOZART [*Brasseur et al.* 1998].

To include hydrogen peroxide limitation effects on SO_4^{2-} production, in-cloud depletion of hydrogen peroxide is calculated according to the last term in (1) together with (5), (6), and (4). Since an interactive simulation of the hydrogen peroxide cycle with respect to photochemistry cannot be realized with sufficient efficiency in complex aerosol models like NARCM, a simple forcing term is used at each grid box to take into account the chemical and physical sources of H_2O_2:

$$\left.\frac{\partial C_{H_2O_2}}{\partial t}\right|_{prod} = -\frac{1}{\tau}\left(C_{H_2O_2} - \overline{C}_{H_2O_2}\right) . \qquad (7)$$

The prescribed background concentration $\overline{C}_{H_2O_2}$ in (7) is supplied from results of the MOZART model. The parameter τ is the timescale of the local H_2O_2 production by photochemical and transport processes in each grid box.

Simulations of the wintertime H_2O_2 production over North America in a photochemical box model showed that production via HO_2 occurs on a time scale of the order of a few hours up to 1 day (P. A. Ariya et al., Major mechanisms for the production of HO, H_2O_2, and organic peroxides during fall and winter: A modeling study, submitted to *Journal of Geophysical Research,* 1999, hereinafter referred to as Ariya et al., submitted manuscript, 1999). Typically, the timescale is shorter in summer due to higher production rates. However, the supply of H_2O_2 is additionally determined by advection and diffusion processes caused by the local wind fields and concentration gradients. As an approximation, $\tau =$ 30 min has been chosen in NARCM to account for these effects. The accuracy of the chosen value can only be tested by comparisons between modeled and observed SO_4^{2-} concentrations and wet deposition fluxes since it is very difficult to derive an optimum value by other means.

2.2. Clear-Sky Condensation and Nucleation

Under continental and clear-sky conditions in the troposphere, particulate sulphate is predominantly formed by condensation of gaseous H_2SO_4 on preexisting aerosol. Over the ocean, H_2SO_4 may also condense on seasalt particles. Another important pathway for the formation of aerosol sulphate is the binary homogeneous nucleation of gaseous H_2SO_4 and water vapor. Both processes are strongly coupled in a highly nonlinear way. To take into account the nonlinearity, the following mass balance for gaseous H_2SO_4 (with $C_{H_2SO_4}$ in molecules cm^{-3}) is solved in NARCM:

$$\frac{dC_{H_2SO_4}}{dt} = k_{SO_2} C_{OH} C_{SO_2} - \sum_i k^i_{cond} C_{H_2SO_4} - g_c k_{nucl} (C_{H_2SO_4})^S . \qquad (8)$$

The first term on the right-hand side in (8) represents the production of H_2SO_4 via gas-phase oxidation of SO_2 by the hydroxyl radical (OH) [*Stockwell and Calvert,* 1983]. In the model, results of the MOZART model are used for C_{OH} [*Brasseur et al.* 1998]. The rate coefficient

k_{SO_2} (in $cm^3\,s^{-1}$) is calculated according to *DeMore et al.* [1992]:

$$k_{SO_2} = \frac{k_0\,M}{1 + k_0\,M/k_\infty}\,F_c^{\left(1+\log^2(k_0\,M/k_\infty)\right)^{-1}},$$

with $k_0 = 3.0 \times 10^{-31}\,(T/300)^{-3.3}$, $k_\infty = 1.5 \times 10^{-12}$, $F_c = 0.6$, and the air density M (in molecules cm^{-3}).

The sum in (8) is over all bins i and represents the production of SO_4^{2-} by condensation of H_2SO_4. The rate constants for the individual bins with the boundaries $\varphi_{i-1/2}$ and $\varphi_{i+1/2}$ are given by

$$k^i_{\rm cond} = 2\,\pi\,D \int_{\varphi_{i-1/2}}^{\varphi_{i+1/2}} D_p\,F({\rm Kn})\,A\,n(\varphi)\,d\varphi\,, \qquad (9)$$

with the diffusivity D of H_2SO_4 in air, the Knudsen number Kn (i.e., the ratio of the mean free path of sulphuric acid in air to the particle radius). The parameter $n(\varphi)$ is the number size distribution of the aerosol. $F({\rm Kn})$ is a coefficient correcting for free molecular effects,

$$F({\rm Kn}) = \frac{1 + {\rm Kn}}{1 + 1.71\,{\rm Kn} + 1.33\,{\rm Kn}^2}\,,$$

and A is a coefficient correcting for the interfacial mass transport limitations described by the accommodation coefficient a_e,

$$A = \left[1 + 1.33\,{\rm Kn}\,F({\rm Kn})\,\left(a_e^{-1} - 1\right)\right]^{-1}\,,$$

with the accommodation coefficient $a_e = 0.02$ [*Russell et al.*, 1994].

The last term in (8) is the nucleation term. The approach used and the parameters g_c, $k_{\rm nucl}$, and S are described in detail in Appendix C.

Equation (8) is solved at each model time step by applying the EBI method described in 2.1.1. The resulting H_2SO_4 concentrations $C^{t+\Delta t}_{H_2SO_4}$ are subsequently used to solve balance equations for the aerosol number size distribution and the sulphate aerosol mass size distribution. Discretisation of the size distributions gives the following prognostic equations for changes in bin particle number concentration N_i (in particles cm^{-3}) and sulphate concentration C_i due to nucleation and condensation:

$$\frac{\Delta N_i}{\Delta t} = \delta_{ij}\,k_{\rm nucl}\,(C^{t+\Delta t}_{H_2SO_4})^S + A^N_{i-1/2} - A^N_{i+1/2}\,, \qquad (10)$$

$$\frac{\Delta C_i}{\Delta t} = \delta_{ij}\,g_c\,k_{\rm nucl}\,(C^{t+\Delta t}_{H_2SO_4})^S + k^i_{\rm cond}\,C^{t+\Delta t}_{H_2SO_4} + A^C_{i-1/2} - A^C_{i+1/2}\,. \qquad (11)$$

The first terms on the right-hand sides in (10) and (11) represents the production of new particles by nucleation in bin $i = 1$, with δ_{ij} being the Kronecker delta and $j = 1$. SO_4^{2-} production by condensation of H_2SO_4 is included by the second term on the right hand side of (11). The last two terms in (10) and (11) take into account the growth of particles due to condensation of H_2SO_4. The calculation of these terms is described in Appendix D.

The results of (10) are used at each EBI time step to evaluate $n(\varphi)$ in the integral (9). A polynomial interpolation is used to take into account the shape of the aerosol number size distribution and the size-dependent parameters in (9) within the bins which allows accurate and efficient simulations with relatively few bins [*von Salzen and Schlünzen*, 1999b]. The calculation of N_i and C_i according to (10) and (11) has the advantage that particle number and total sulphate mass are both conserved for H_2SO_4 condensation which is not necessarily the case in other aerosol growth models [e.g., *von Salzen and Schlünzen*, 1999a].

3. Simulation of Sulphate Aerosol Over North America

The response of sulphate aerosol concentrations and sizes to changing SO_x emissions and H_2O_2 concentrations may strongly depend on the region and the season owing to regional and seasonal dependencies of the emissions and the physical and chemical processes. Over North America the efficiency of sulphate production is higher in summer than in winter due to increased photochemical production of oxidants. However, compared to clear-sky production of SO_4^{2-}, the in-cloud aerosol production is relatively more important in winter [*Roelofs et al.*, 1998].

To test the model for North America at two different seasons, the model was run for the periods July 17 to 30, 1994, and December 6 to 19, 1994, according to the model configuration described in section 2. The results have been averaged over these periods to compare model results with meteorological and chemical observations which are available for these periods. The same periods are subsequently used to study the sensitivity of the results to an artificial overall decrease in anthropogenic SO_x emissions by 50%. Additionally, responses to an artificial overall increase in H_2O_2 background concentrations by 100% are studied. No other modifications are made in the sensitivity tests.

No single 2-week period can be truly representative of the season climatology. Nevertheless, to obtain a rough qualitative assessment of how well the meteorology of these periods corresponds to climatology, we compared the meteorological situations with mean climatological values for July and December. Results of the NCEP/NCAR Reanalysis Project [*Kalnay et al.*, 1996] for the simulation periods and for the climatological situations for the years 1961 to 1990 give evidence for similar pressure systems with low sealevel pressure over the continent and high pressure over the ocean in July and high sealevel pressure over the continent in December. However, the magnitudes and exact locations of the troughs and ridges are slightly different. The

bias in ground-level temperature is relatively small with differences below 1 K for most regions. The amounts and regional patterns of the precipitation in July show some characteristic differences. For the eastern United States the mean precipitation rate during the simulation period is about 50% higher than the climatological value. However, only small differences in precipitation rates occur for December (less than 3% difference in the mean values for the eastern United States).

3.1. Initialization and Boundary Conditions

The simulations include windspeed and size-dependent emissions of seasalt by the ocean. The approach and applications have been presented by *Gong et al.* [1997a, b].

Anthropogenic emissions of SO_2 and SO_4^{-2} are provided by the GEIA 1985 1-B inventory [*Benkovitz et al.*, 1996], which has two levels and four seasons. For emissions from point sources, the plume rise formulation of *Briggs* [1975] is applied to take into account the effects of atmospheric stability on the effective heights of the sources. The 1985 emissions are adjusted to account as well as possible for changes in emissions between 1985 and 1994. The emission scale factor used in the adjustment ranges from 0.97 for the southeastern United States to 0.70 for the northeastern United States. For Canada, values of the scale factor range from 0.42 for Ontario to 1.29 for Newfoundland (Spacek et al., submitted manuscript, 1999).

For natural emissions of H_2S the $1°\times1°$ resolution surface flux inventory of *Bates et al.* [1992] is used. For emissions of DMS by the ocean a $1°\times1°$ resolution oceanic surface concentration inventory [*Kettle et al.*, 1999] is used to compute the DMS flux by a mass transfer scheme.

The removal of SO_2 from the model ground level by dry deposition is parameterized according to *Padro et al.* [1991]. For aerosol particles the approach described by *Gong et al.* [1997a] is used. Concentrations of the tracers are set to zero at the lateral boundaries and at the beginning of the simulation. The model spin-up time before the start of the analyzed simulation periods is 1 week.

The lateral boundary values for meteorological variables are provided within a sponge zone at the boundaries of the model domain using NMC/NCEP operational analysis data which are provided every 12 hours in the model. The sea surface temperatures are obtained from monthly climatological fields.

3.2. Results for Summer 1994

For a comparison of the mean model results during the simulation period, mean sealevel pressure, wind fields, and relative humidity provided by NMC/NCEP analysis are shown in Figures 1a and 1c. The corresponding model results are shown in Figures 1b and 1d. Additionally, Figure 1e shows World Meteorological Organization (WMO) observations of mean daily precipitation at 910 meteorological stations. The simulated precipitation rate is shown in Figure 1f. Owing to a limited number of stations over ocean and over Canada, the results in Figure 1e are less reliable in these regions. Thus the discussion of the model performance focuses only on the precipitation results over the United States.

The meteorological situation during the period is characterized by low pressure over the Rocky Mountains and over the Hudson Bay (Figure 1a). Over the United States Midwest and eastern North America, westerly winds prevail while southerly winds are dominant at the Atlantic coast and over the Gulf of Mexico. As a result of the transport of marine air masses to southeastern and eastern North America, the relative humidity exceeds 80% in some regions (Figure 1c). These regions are also characterized by high precipitation (Figure 1e).

The mean modeled sealevel pressure field compares well with the analysis (compare Figure 1a with Figure 1b). However, differences in magnitude and direction of the winds at the Atlantic coast cause too much inflow of marine air to eastern North America. Differences between modeled and observed relative humidity over North America may be in part attributed to an insufficient spin-up time of the model since the lower boundary conditions are sensitive to the initial values of the soil moisture properties which are provided as climatological means in the simulation (Spacek et al., submitted manuscript, 1999). This may also explain some of the differences between modeled and observed precipitation. In conclusion, the model tends to underpredict relative humidity and precipitation over southeastern North America.

A comparison of mean modeled concentrations and observed SO_4^{2-} concentrations from the Clean Air Status and Trends Network (CASTNet) and the Canadian Air and Precipitation Monitoring Network (CAPMoN) shows good agreement (Figures 2a and 2b). The mean concentrations are 13% lower in the simulation, compared to a mean observed concentration of 6.4 $\mu g\,m^{-3}$. Additionally, the mean wet deposition is 23% lower in the model (Figures 2c and 2d). These results give evidence that the production of sulphate over eastern North America is slightly underestimated in the simulation.

Differences in the production rates of SO_4^{2-} over eastern North America are mainly caused by differences in the meteorological situations between model and observations. For example, the stronger inflow of relatively unpolluted marine air at the Atlantic coast in the simulation causes too low SO_4^{2-} concentrations in this region compared to the observations. This is also the cause for the relatively low mean wet deposition of SO_4^{2-} in this region (compare Figures 2c and 2d). The underestimation of wet deposition in the southeastern part of the model domain is mostly caused by too little modeled precipitation in this region.

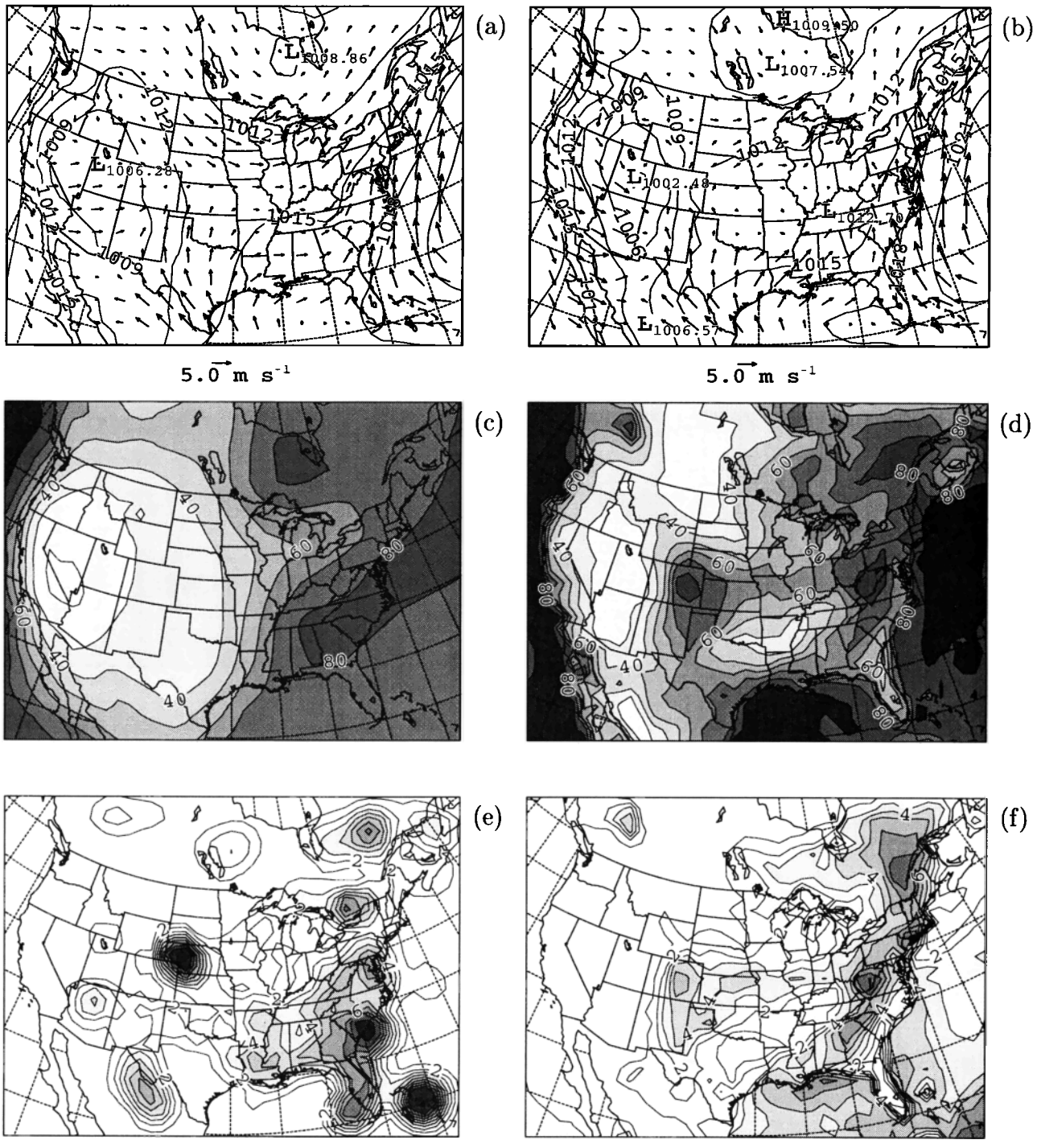

Figure 1. Comparison of observed (left column) and simulated (right column) meteorological variables for July 17 to 30, 1994. (a) and (b) Wind fields at the ground level (in $m\,s^{-1}$) and sealevel pressure (in hPa), (c) and (d) relative humidity at the ground level (in %), and (e) and (f) precipitation (in $mm\,d^{-1}$).

In contrast to the good agreement between modeled and observed SO_4^{2-}, there are substantial differences for SO_2 (Figure 3). The model overpredicts the mean SO_2 concentrations at the ground by 185% for eastern North America. The overpredictions may give evidence for too strong vertical mixing in the PBL in the model. Additionally, it is very likely that the differences result from the relatively low resolution of the model over the source regions. In the model, sulphur dioxide may either be emitted into the lowest model level or into higher model levels, depending on stack heights, emission rates and the meteorological situation (section 3.1). Compared to the actual situation with typically much narrower plumes, the distribution of the

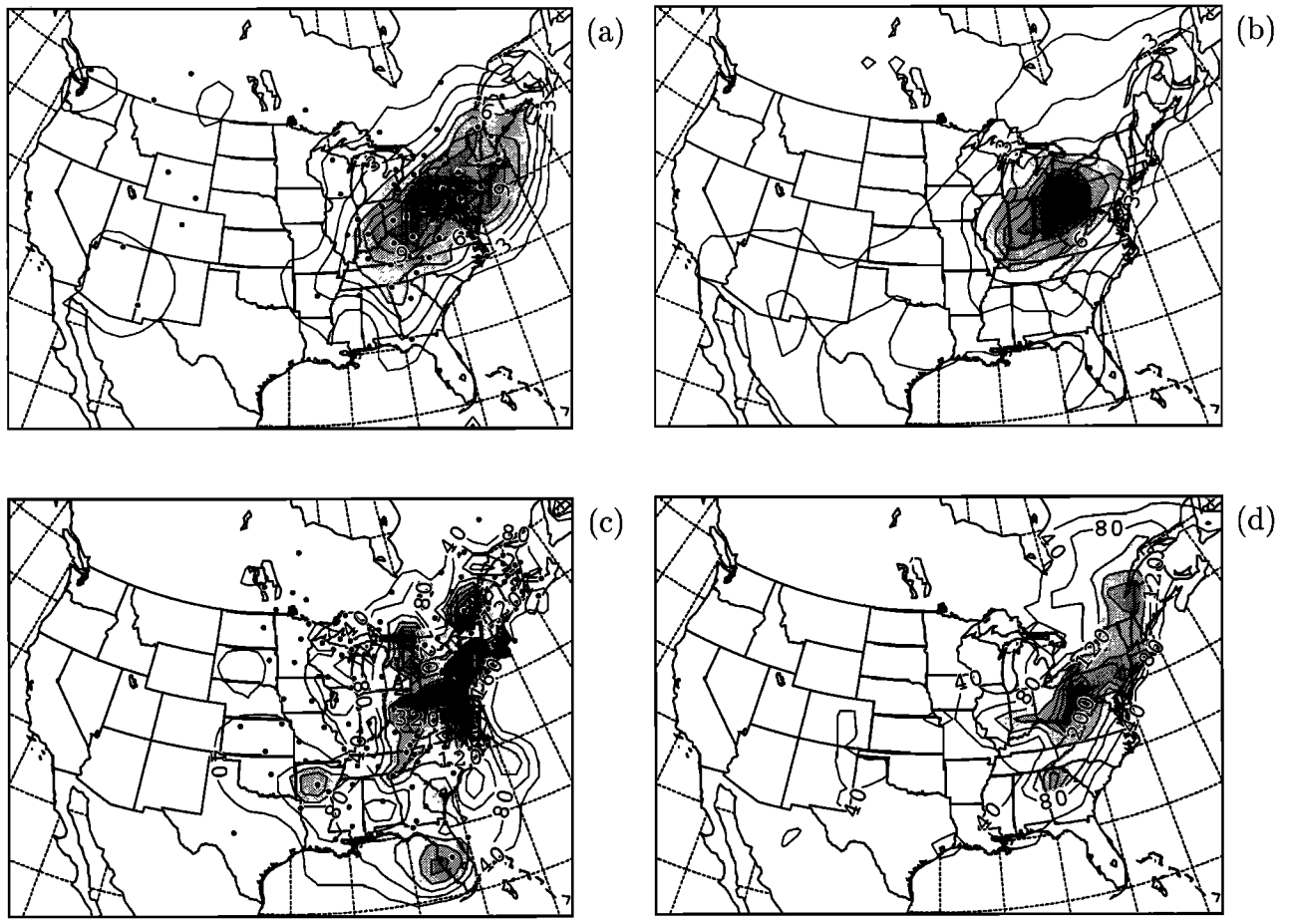

Figure 2. Comparison of observed (left column) and simulated (right column) sulphate concentration and wet deposition for July 17 to 30, 1994. (a) and (b) Sulphate concentrations at the ground level (in $\mu g\,m^{-3}$) and (c) and (d) sulphate wet deposition (in $g\,ha^{-1}\,d^{-1}$). For the observations the locations of the observation stations are also shown in Figures 2b and 2d.

emissions over the large model grid box volumes represents an artificial and much too strong mixing of the sulphur dioxide plumes with ambient air near emission sources. Thus too much SO_2 is vertically advected and diffused from the emission grid box to the ground level. This causes unrealistic high concentrations in the entire layer from the ground up to the emission grid box. Although the ground level concentrations are clearly not realistic, the concentrations further downwind from the sources and the column integrated concentrations can be expected to be more reasonable. Results of *Karamchandani and Peters* [1983] and *Kasibhatla and Peters* [1990] give evidence that there is in fact need for parameterizations of subgrid-scale plumes in regional and global models. However, only relatively few parameterizations have been suggested, and they have been applied to only a very limited number of cases [*Seigneur et al.*, 1993; *Bigalke*, 1992].

A major goal of NARCM is to simulate aerosol size distributions. As an example, Figure 4 shows the average simulated mass mean diameter of the sulphate aerosol at the ground. It appears that there are substantial differences between the results over land and over sea.

Over land the highest values of the mass mean diameter occur in regions with high SO_x emissions and in regions with high relative humidity and precipitation. The lowest values are predicted over relatively remote regions such as the Rocky Mountains. The spatial distribution in Figure 4 gives evidence for the importance of aerosol growth by oxidation of reduced sulphur species over the source regions and by uptake of water vapor in regions with high relative humidity. A qualitative comparison of the mass mean diameters over land with the in-cloud oxidation rates of SO_2 gives evidence for a strong correlation between aerosol size and in-cloud SO_4^{-2} production even though in-cloud oxidation contributes less than 50% to the total SO_4^{2-} production over the United States in this particular simulation (not shown).

In contrast, the aerosol sizes over the ocean are mainly determined by clear-sky processes. The mass mean diameter obtained for the SO_4^{2-} size distribution near the northeastern coast of the United States is sim-

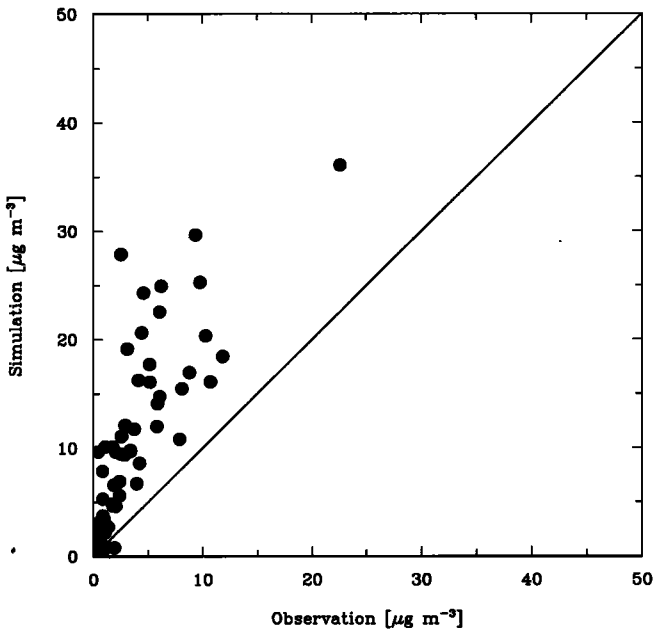

Figure 3. Comparison of simulated and observed SO_2 concentrations at the ground level at CASTNet stations for July 17 to 30, 1994.

ilar to the mass mean diameter obtained for the seasalt size distribution (Figure 4). The relatively high concentrations of sulphate in seasalt containing particles are caused by efficient uptake of H_2SO_4 on seasalt aerosol above the sea surface.

Unfortunately, no observations of particle sizes are available during the simulation period. Thus the simulation results cannot be tested directly. Instead, model results for sulphate aerosol are compared to observed aerosol number size distributions taken during three summer experiments at different locations over the eastern United States. The first data set was taken during the PRECP V Experiment which involved 12 flights during the time period June 2 to 23, 1987, over Ohio [*Kleinman and Daum,* 1991a]. The aerosol size distribution was measured with an Active Scattering Aerosol Spectrometer Probe (ASASP) with 15 size classes between 0.12 and 2.9 μm particle diameter. The other data sets were taken during the New York City (NYC) Urban Plume Experiment from July 1 to 28, 1996 over New York [*Kleinman et al.,* 2000] and during the Southern Oxidants Study (SOS) from June 24 to July 20, 1995, over Tennessee [*Hubler et al.,* 1998]. Data from 15 and 17 flights, respectively, are available for these two experiments. In both experiments a Passive Cavity Aerosol Spectrometer Probe (PCASP) was used to sample the aerosol number size distribution between 0.1 and 3.5 μm particle diameter in 15 size classes.

The experimental designs of all three experiments were to sample over a wide range of conditions so as to capture the contrast between relatively polluted episodes and intervening cleaner periods. This strategy and the duration of the sampling periods implies that the mean results of the experiments can be usefully compared to the model results. In detail, comparisons of the meteorological situations from results of the NCEP/NCAR Reanalysis Project for the periods of the individual experiments and the simulation give evidence for good agreement in terms of meteorological parameters. The periods of the simulation and the experiments are all characterized by low sea level pres-

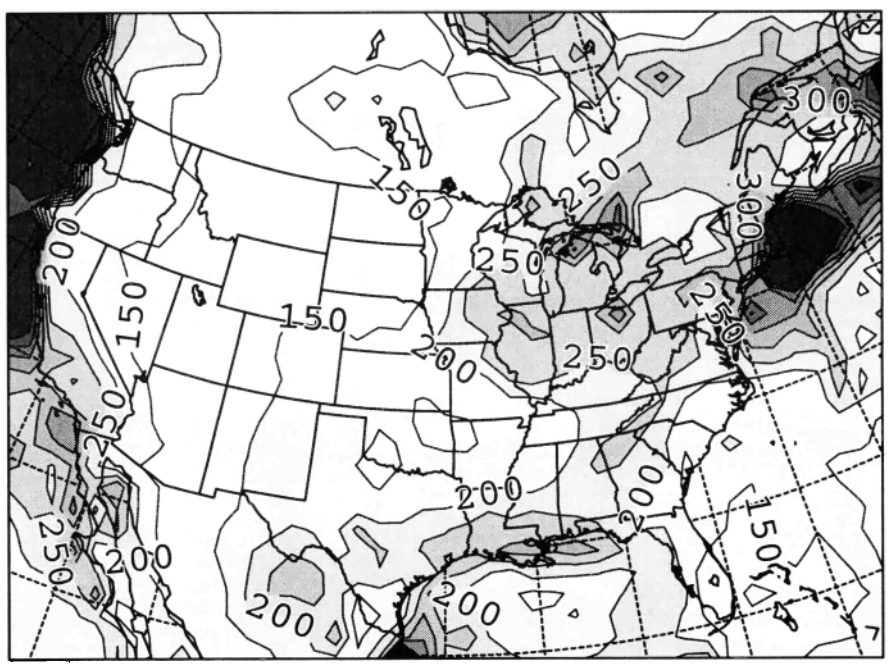

Figure 4. Simulated mass mean diameter of sulphate aerosol at the surface for July 17 to 30, 1994 (in nm).

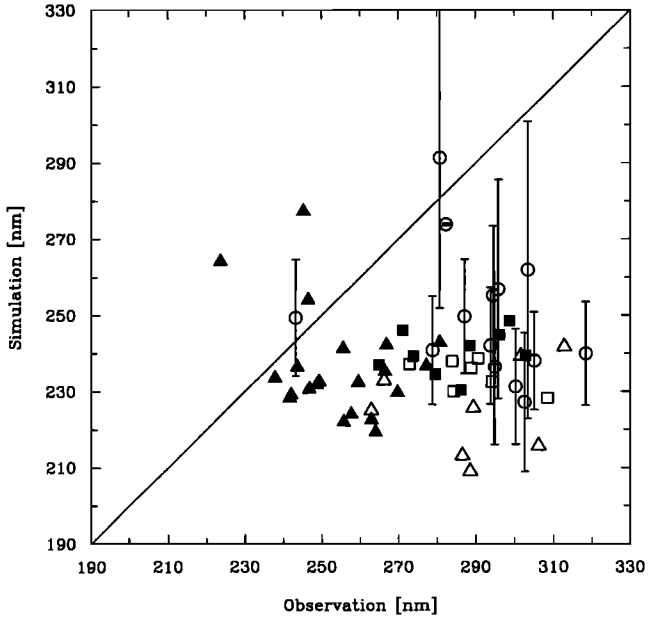

Figure 5. Comparison of mean simulated and observed aerosol mass mean diameters in layers ranging from the ground to 850 hPa (solid markers) and from 850 hPa to 250 hPa (open markers) at corresponding individual horizontal model grid points. Results from the New York City Urban Plume Experiment are marked by triangles, results from the Southern Oxidants Study are marked by squares, and results from the PRECP V Experiment are marked by circles. The uncertainties in the PRECP V data due to the unknown heating of the probe are indicated by error bars.

sure over northeastern Canada and high pressure off the Atlantic coast. Whereas differences in ground level temperatures are small (i.e., less than 1 K over the eastern United States), biases in precipitation rates are more pronounced. Although the maximum in precipitation is situated over the southeastern United States for all periods, there are slight differences in the regional distributions. For example, the reanalysis results give evidence for about one fifth (for the SOS) to one third (for the PRECP V Experiment) less precipitation for the eastern United States than in the simulation period.

To compare simulated sulphate mass size distributions with the observed number size distributions, first mass size distributions have been calculated from the observations assuming spherical sulphate particles and constant aerosol densities throughout the entire range of considered particle sizes. A particle size range from 0.12 to 1.24 μm has been selected in order to minimize the influences of aerosol with small sulphate contents on the results. The individual derived mass size distributions have been assigned to the nearest horizontal grid box of the model according to the locations at which the observations were made during the various flights. In the vertical direction the values have been grouped according to two layers, one ranging from the ground to 850 hPa, the other from 850 hPa to 250 hPa. Finally, grid cell averaged and layer-averaged values of the derived mass size distributions are used to obtain mass mean diameters and standard deviations to characterize the observed aerosol size distributions and to make comparisons with model results for individual horizontal grid points and the two layers. Only clear-sky situations are considered in the comparisons of observations and model results.

Since heating was applied to the aerosol sampled by the PCASP, it is assumed that the results are representative of a dry aerosol size distribution. However, it is not clear if sufficient heating to completely dry the aerosol was applied to the ASASP samples. To estimate the uncertainties associated with the unknown heating in the ASASP, the ASASP results are compared to both the dry simulated sulphate aerosol and also the wet aerosol at simulated ambient relative humidity.

Figure 5 shows a comparison of the simulated mass mean diameters and observations in the two layers. For the PRECP V Experiment, only results in the upper layer are shown due to insufficient sampling times in the lower layer. The results in both layers are similar in magnitude and variance. In the lower layer the mean modeled value (238 nm) is 10% smaller than the observed value (263 nm). In the upper layer the mean simulated value is 15 to 21% smaller, depending on the assumption of dry or wet particles in the simulation.

A comparison of the standard deviations of the size distributions shows that the simulated size distributions are slightly broader than the observed size distributions (Figure 6). In the lower layer, the mean standard deviation of the simulated size distributions is 14% higher than that of the observed ones. In the upper layer, the difference is 7 to 11%.

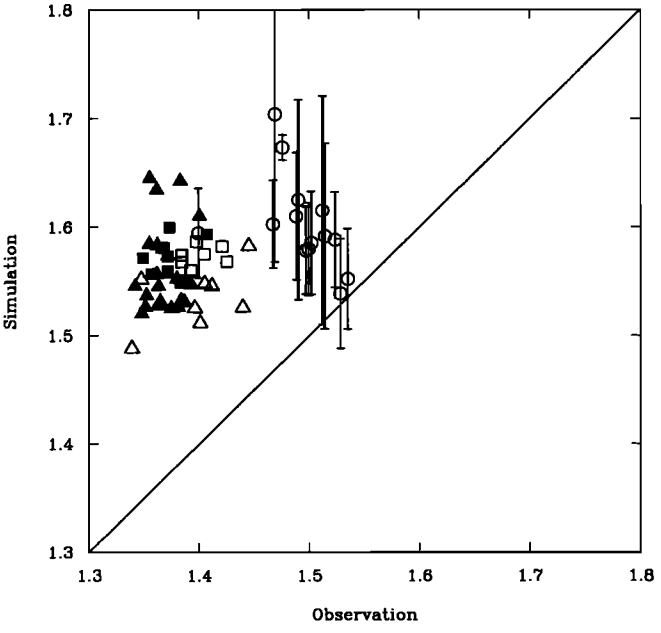

Figure 6. The same as Figure 5 for a comparison of simulated and observed aerosol standard deviations.

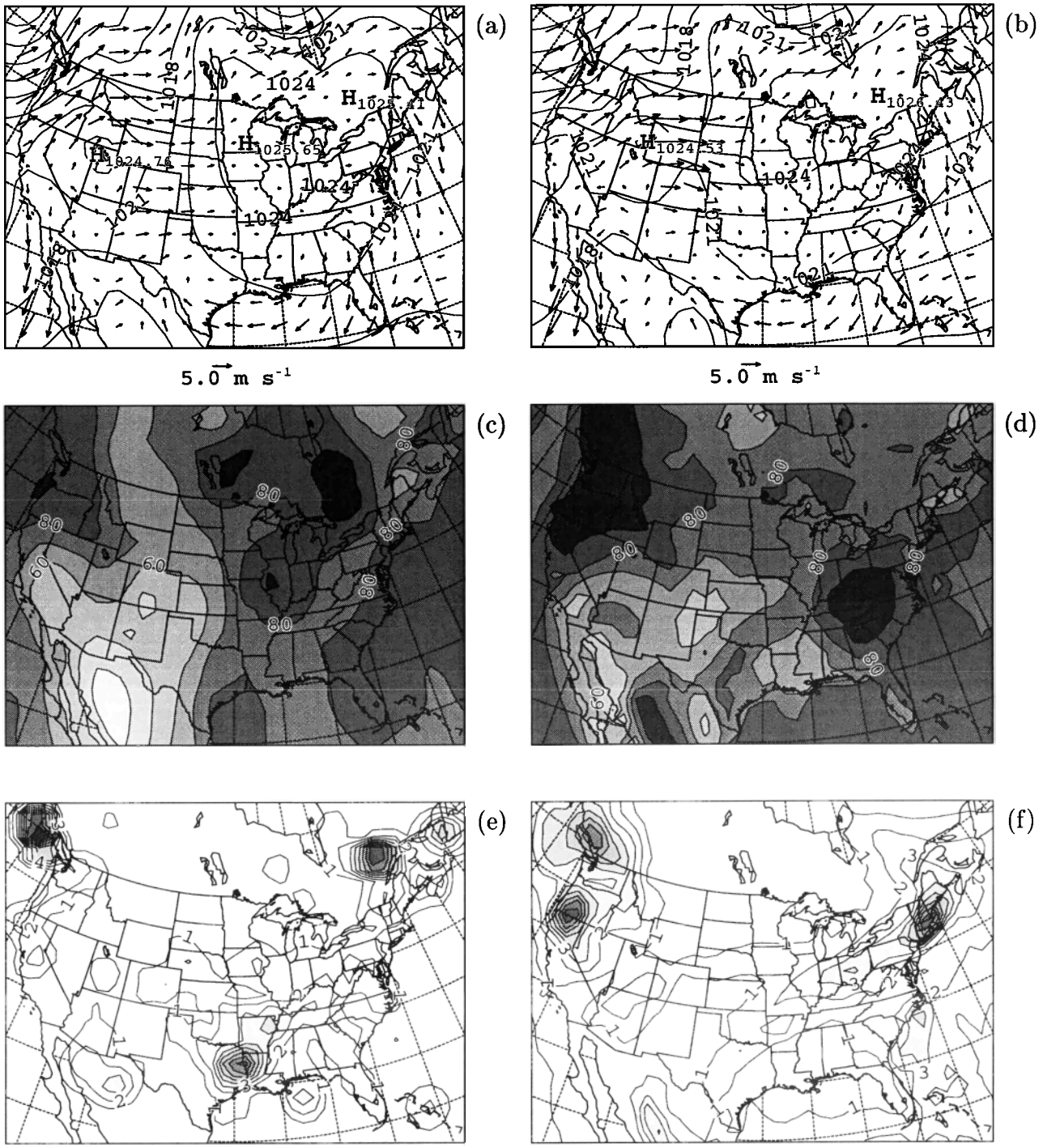

Figure 7. The same as Figure 1 for aerosol during the time period December 6 to 19, 1994.

There are several possible explanations for the differences between simulated sulphate mass mean diameters in NARCM and values derived from observations of tropospheric aerosols (Spacek et al., submitted manuscript, 1999). In this particular simulation the relatively small values of the mass mean diameters can probably be attributed to the omission of aerosol compounds other than sulphate such as organics. At least some fraction of the additional aerosol compounds can be assumed to exist in an internal mixture with sulphate. The omission of these compounds in NARCM means that NARCM tends to underestimate aerosol sizes in regions where aerosol compounds other than sulphate are important.

3.3. Results for Winter 1994

Contrary to the meteorological situation during the July period, the time period December 6 to 9 is char-

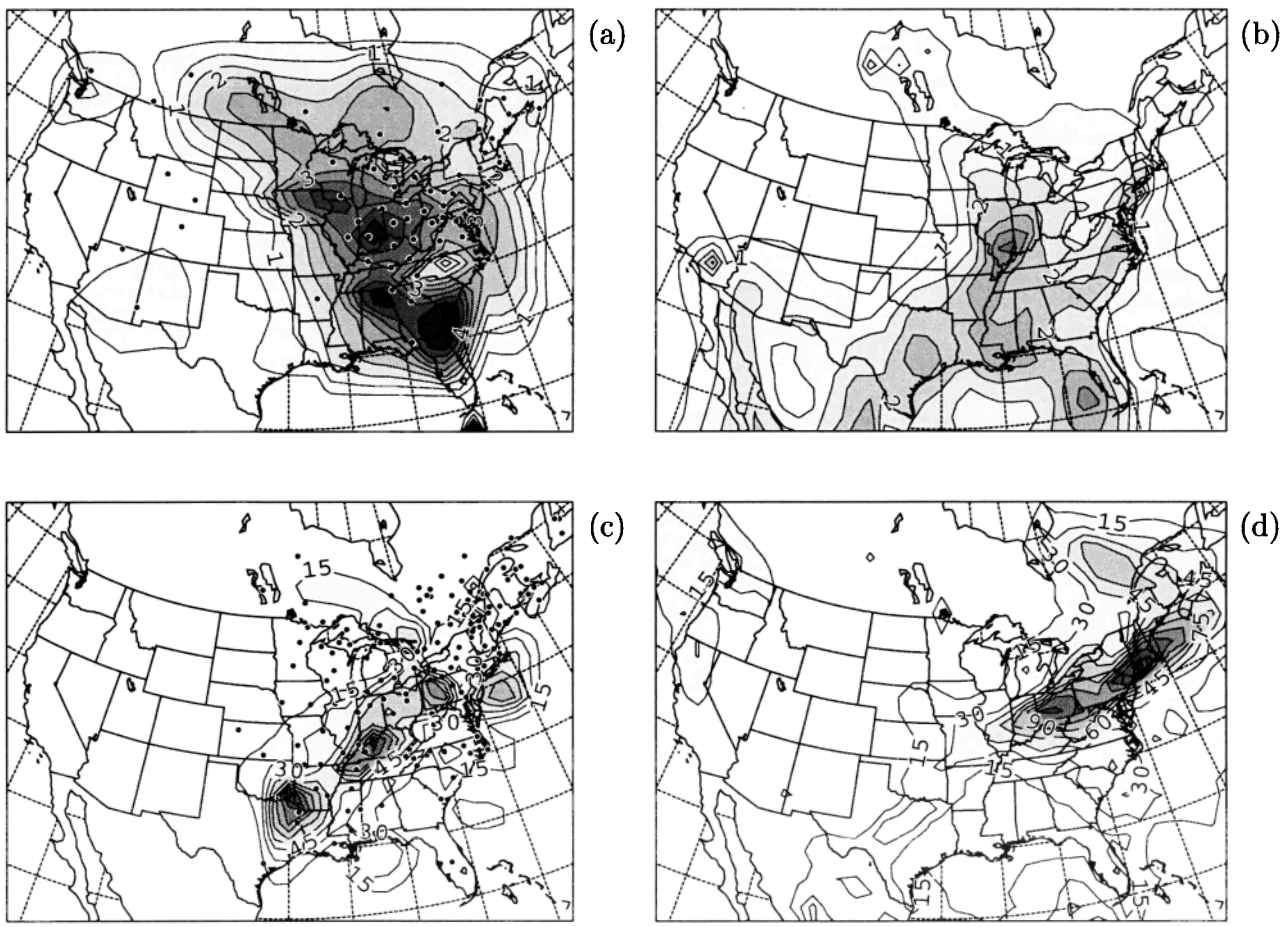

Figure 8. The same as Figure 2 for aerosol during the time period December 6 to 19, 1994.

acterized by high-pressure systems centered over the Rocky Mountains and adjacent to the Great Lakes (Figure 7a). Consequently, northerly and northeasterly winds over the Atlantic coast and in some regions over eastern North America were analyzed.

The simulation results are in good agreement with the NMC/NCEP analysis (Figure 7b). Differences in direction and magnitude of the wind are small. However, there are considerable differences between observed and modeled relative humidity (Figures 7c and 7d) and precipitation (Figures 7e and 7f). Whereas high precipitation was observed over the lower United States Midwest, only very small amounts are simulated in this region. In contrast, much higher precipitation is simulated over the United States Northeast compared to the observations.

Compared to the results for the July period, the SO_4^{2-} concentrations are relatively low (Figure 8a). The mean concentration for all network stations is 2.5 $\mu g\,m^{-3}$. Relatively low values were also observed for the sulphate wet deposition (Figure 8c).

The mean simulated SO_4^{2-} concentration at the locations of the network stations is 46% lower than the observed value. The location of the concentration maximum corresponds well in both results (Figure 8a and 8b). Owing to low network coverage in the United States Southeast and Midwest, more detailed comparisons of the spatial distributions of SO_4^{2-} are not very meaningful. In contrast to the lower simulated mean SO_4^{2-} concentrations, the mean sulphate wet deposition is overpredicted by 54% in the simulation. These results suggest that the low SO_4^{2-} concentrations in the simulation may be at least in part caused by too much SO_4^{2-} wet deposition. This is supported by the mean precipitation at the WMO network stations which is also 54% higher in the simulation. At least some of the differences between simulated and observed SO_4^{2-} wet deposition patterns (Figures 8a and 8b) can be explained by differences in precipitation (Figure 7e and 7f). Additionally, discrepancies between modeled and observed concentrations may be caused by differences in the oxidant concentrations. Comparisons of modeled H_2O_2 concentrations with observations off the coast of Asia by *Hauglustaine et al.* [1998] give evidence for too low H_2O_2 concentrations in MOZART during fall and winter. Recent results of box model studies (Ariya et al., submitted manuscript, 1999) suggest that current model approaches for H_2O_2 production may be too sim-

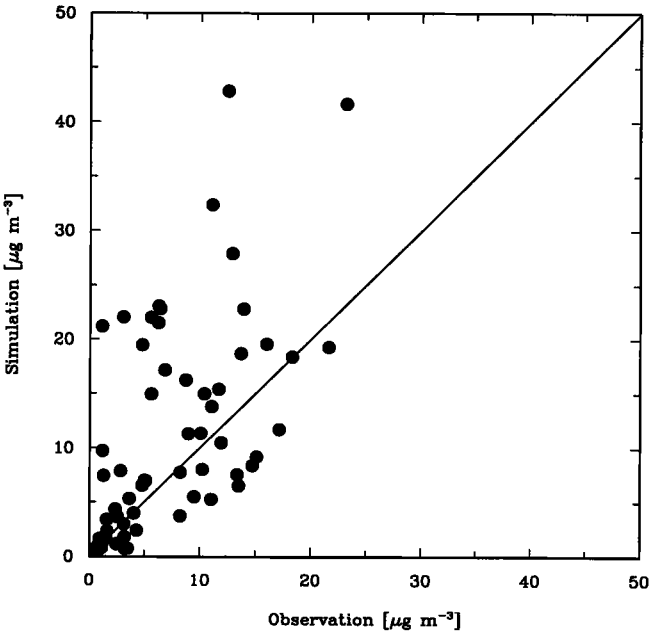

Figure 9. The same as Figure 3 for SO_2 concentrations during the time period December 6 to 19, 1994.

ple since they do not fully consider ozonolysis reactions. The results suggest that direct OH and H_2O_2 production by ozonolysis of alkenes may serve as the major tropospheric source of these oxidants during winter and fall at mid and high latitudes over the continents.

Observed and simulated SO_2 concentrations are both higher than in summer (Figure 9). The simulated mean concentration at all network stations is 53% higher than the observed value of 7.2 $\mu g\,m^{-3}$.

The SO_4^{2-} aerosol particles are larger than during the July simulation period (Figure 10). This is primarily attributable to higher relative humidities during this period. Compared to July, values of the mass mean diameter of the dry SO_4^{2-} aerosol are similar (not shown).

4. Effects of Changing SO_x Emissions and H_2O_2 Concentrations

The simulation results presented in the previous section are used to study the effects of relative changes in SO_x emissions and H_2O_2 background concentrations on the sulphate aerosol during the simulation time period. Specifically, the sensitivity of the results to a homogeneous decrease in anthropogenic SO_x emissions over land by 50% and to a 100% increase in H_2O_2 background concentrations is investigated.

The sensitivity studies are idealized in the sense that they neglect feedbacks of changes in SO_2 concentrations on the gas phase production of H_2O_2. It has been shown that decreases in SO_2 concentrations may lead to decreases in H_2O_2 production because the HO_x equilibrium in the gas phase shifts towards lower HO_2 radical concentrations at lower SO_2 concentrations [*Stockwell*, 1994]. Small changes in HO_2 radical concentrations lead to larger changes in the rate of H_2O_2 production since the formation rate of H_2O_2 depends upon the square of the HO_2 concentrations. However, the effects of changes in SO_2 concentrations on H_2O_2 concentrations are likely small in our simulations and can be neglected.

4.1. Results for Summer 1994

Figure 11 shows the relative changes in sulphate concentrations at the surface (Figures 11a and 11b), sulphate wet deposition (Figures 11c and 11d), and sul-

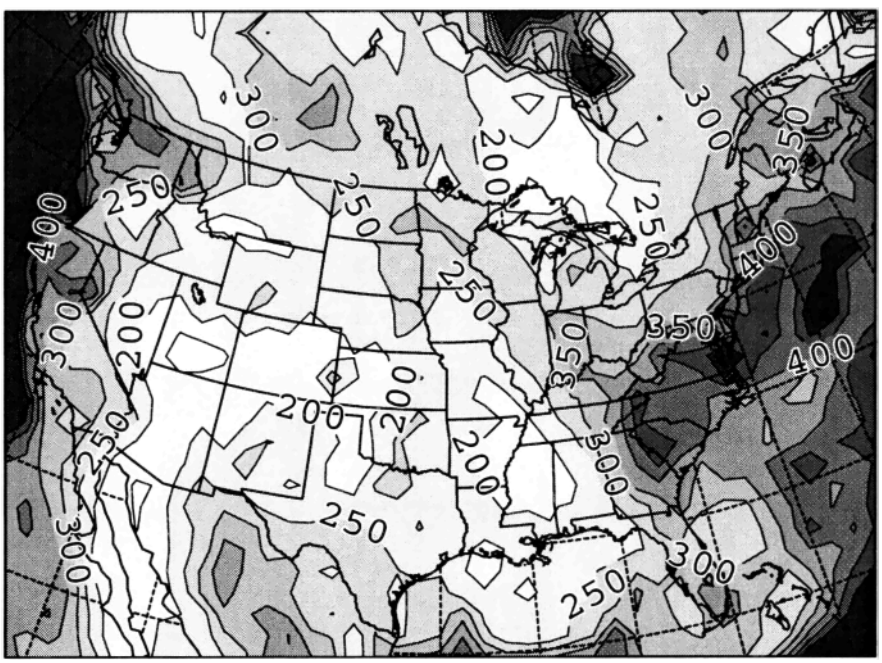

Figure 10. The same as Figure 4 for aerosol during the time period December 6 to 19, 1994.

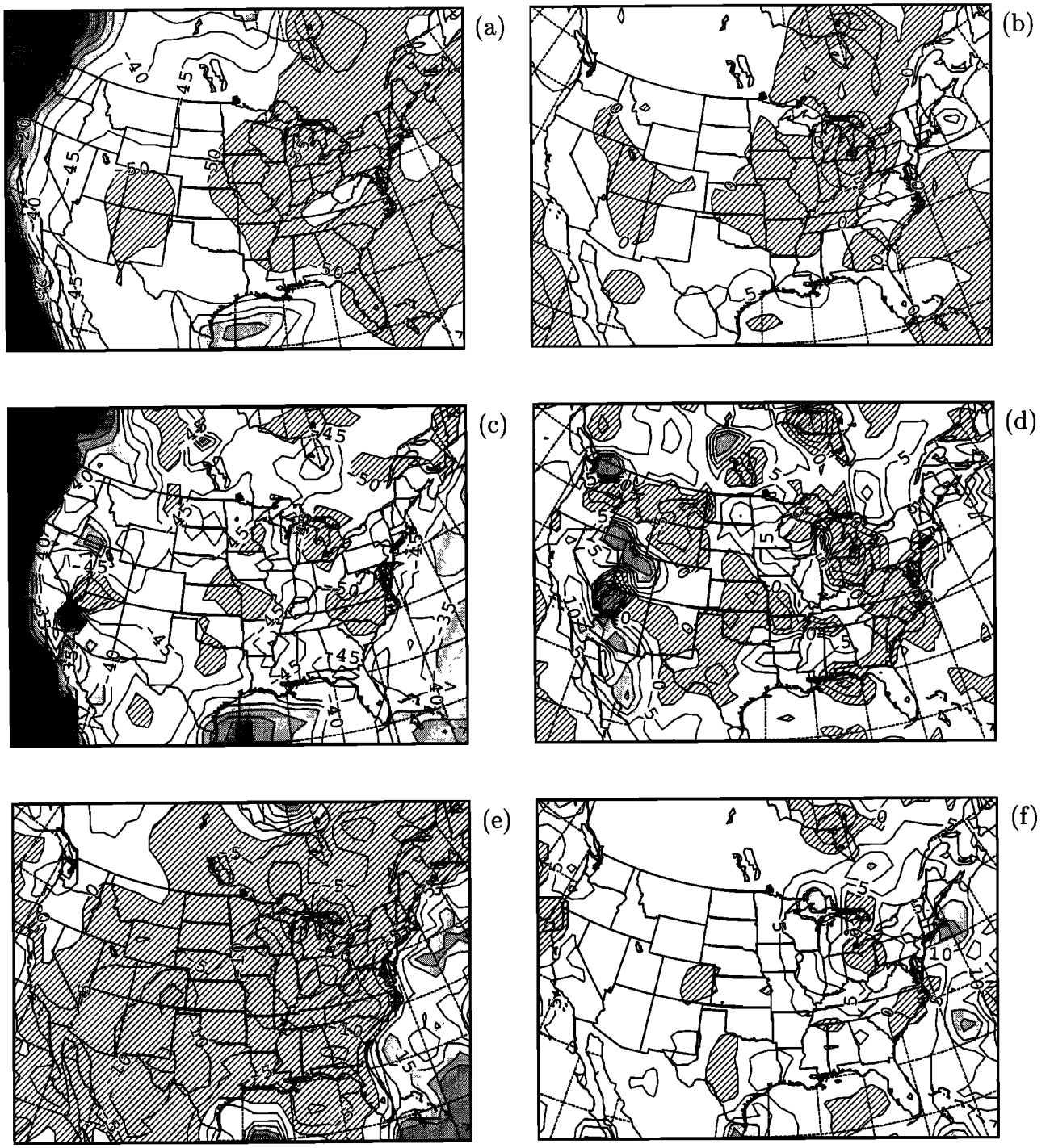

Figure 11. Effects of changing SO_x emissions (left column) and H_2O_2 background concentrations (right column) on sulphate aerosol during the time period July 17 to 30, 1994. (a) and (b) Relative changes (in 5% intervals) of sulphate concentrations at the ground, (c) and (d) sulphate wet deposition, and (e) and (f) sulphate aerosol mass mean diameter at the ground. Areas with deviations of less than -50% (Figures 11a and 11c) and deviations of less than 0% (Figures 11b, 11d, 11e, and 11f) are hatched.

phate aerosol mass mean diameter at the surface (Figures 11e and 11f) due to decreased SO_x emissions (left column in Figure 11) and increased H_2O_2 background concentrations (right column in Figure 11). The results in this figure have been smoothed by a nine gridpoint filter to reduce fluctuations in the results. These fluctuations are mainly caused by local modifications in cloud cover due to the feedback of aerosol concentrations on stratiform cloud microphysics (see section 2).

On average, a 50% decrease in SO_x emissions results in an approximately similar response in sulphate concentrations (Figure 11a) and a slight nonlinear response

of sulphate wet deposition (Figure 11c) over land. The mass mean diameter decreases by about 5 to 10% over regions with relative abundant sulphate concentrations (Figure 11e). Over sea the changes are smaller since emissions of DMS are not modified in the sensitivity tests.

The approximately linear responses of aerosol concentrations and sulphate wet deposition to changes in SO_x emissions give evidence that the in-cloud production of SO_4^{2-} is not significantly limited by insufficient H_2O_2 concentrations. Changes in aerosol size are caused by nonlinear decreases in aerosol number concentrations. Owing to disproportional decreases in aerosol nucleation rates, the column integrated aerosol number concentration decreases by about 30 to 40% over eastern North America and by about 10 to 20% over the southwestern United States. Consequently, decreases in the ratios of aerosol mass to aerosol number concentrations in the simulation result in a decrease in aerosol particle sizes over most of North America. Over the sea surface, increases in sulphate mass mean diameters are explained by condensation of H_2SO_4 on seasalt aerosol which becomes more important at reduced accumulation mode aerosol concentrations due to decreased SO_x emissions.

Changes in H_2O_2 background concentrations have only relatively small effects on the SO_4^{2-} concentrations at the ground (Figure 11b). The most significant change is a decrease in sulphate concentrations over the northern part of eastern North America by a few percent. Figure 11d shows that the sulphate wet deposition also tends to decrease slightly in this region but tends to increase elsewhere. Similar trends occur for the sulphate aerosol mass mean diameter (Figure 11f). Changes in aerosol number concentrations are also less than a few percent.

The fairly small responses of sulphate wet deposition to changes in H_2O_2 background concentrations and the almost linear responses to changes in SO_x emissions give evidence that the in-cloud production of sulphate aerosol during the simulation time period is mainly limited by the available amounts of SO_2 in the clouds. In contrast, other studies based on measurements of SO_2 and H_2O_2 concentrations over eastern North America in summer give evidence that limitation of in-cloud production due to SO_2 may not be very important in comparison to limitations due to H_2O_2 [*Meagher et al.*, 1984; *Kleinman and Daum,* 1991a]. However, as *Kleinman and Daum* [1991b] pointed out, SO_2 concentrations may be considerably less than H_2O_2 concentrations at higher altitudes, and SO_2 limitation at these altitudes is therefore more important as it is at lower altitudes. In agreement with the observations, the simulation results show lower H_2O_2 in-cloud concentrations at low altitudes compared to SO_2 and the opposite at altitudes above about 850 hPa. Additionally, the simulation gives evidence that H_2O_2 may be less important as an oxidant over the source regions than is assumed in the observational studies. In the simulation it appears that the total, column integrated in-cloud oxidation of SO_2 by ozone is of similar importance over the source regions to that by H_2O_2. This is also true in other regions, where O_3 concentrations are high and H_2O_2 concentrations are low compared to average background concentrations over North America. In the simulation, more than 50% of the total in-cloud oxidation occurs in convective clouds, and oxidation in stratiform clouds appears to be less important due to low stratiform cloud amounts in the simulation. In the convective updrafts the SO_4^{2-} production by O_3 occurs at higher altitudes than the in-cloud production by H_2O_2 and tends to almost completely oxidize the SO_2 that was not already oxidized by H_2O_2 at lower altitudes. The increasing relative importance of O_3 with increasing height can be in part explained by the decreasing importance of H_2O_2 with height due to depletion of H_2O_2 by in-cloud oxidation and insufficient supply by entrainment. Another cause is the simulated increase in cloud water pH from about 3.5 above ground to about 5 at 200 hPa due to relatively low SO_4^{2-} concentrations and still considerable ammonia concentrations at high altitudes [e.g., *Dentener and Crutzen,* 1994]. Since the oxidation of SO_2 by O_3 depends strongly on the pH, the oxidation of SO_2 by O_3 is much more efficient at the high simulated pH values at higher altitudes.

The relatively small decreases in SO_4^{2-} concentrations, wet deposition, and mass mean diameter over some regions in eastern North America due to increased H_2O_2 background concentrations are mainly caused by decreased cloud amounts over these regions due to feedback of aerosols on stratiform cloud microphysics. Eventually, changes in stratiform cloud amounts and precipitation affect in-cloud oxidation in convective clouds in the simulation. These changes have only minor effects on the average results since decreases in cloud amounts and in-cloud oxidation in some regions are associated with increases in other regions, for example, in some parts of the Midwest.

4.2. Results for Winter 1994

A reduction in anthropogenic SO_x emissions results in a similar change in SO_4^{2-} concentrations (Figure 12a) and aerosol number concentrations. However, the SO_4^{2-} wet deposition responds in a clearly nonlinear way (Figure 12c). Reductions of only up to 35% are simulated over the source regions in eastern North America. Changes in the mass mean diameter are small (Figure 12e).

Although the nonlinear responses of SO_4^{2-} wet deposition for eastern North America give evidence for nonlinear responses of SO_4^{2-} in-cloud production rates, this hardly effects the SO_4^{2-} concentrations since the in-cloud production accounts for less than 50% of the total SO_4^{2-} production over the southeastern United States. In contrast, the contribution of clouds to the total SO_4^{2-} production is of the order of 80 to 90% over the North

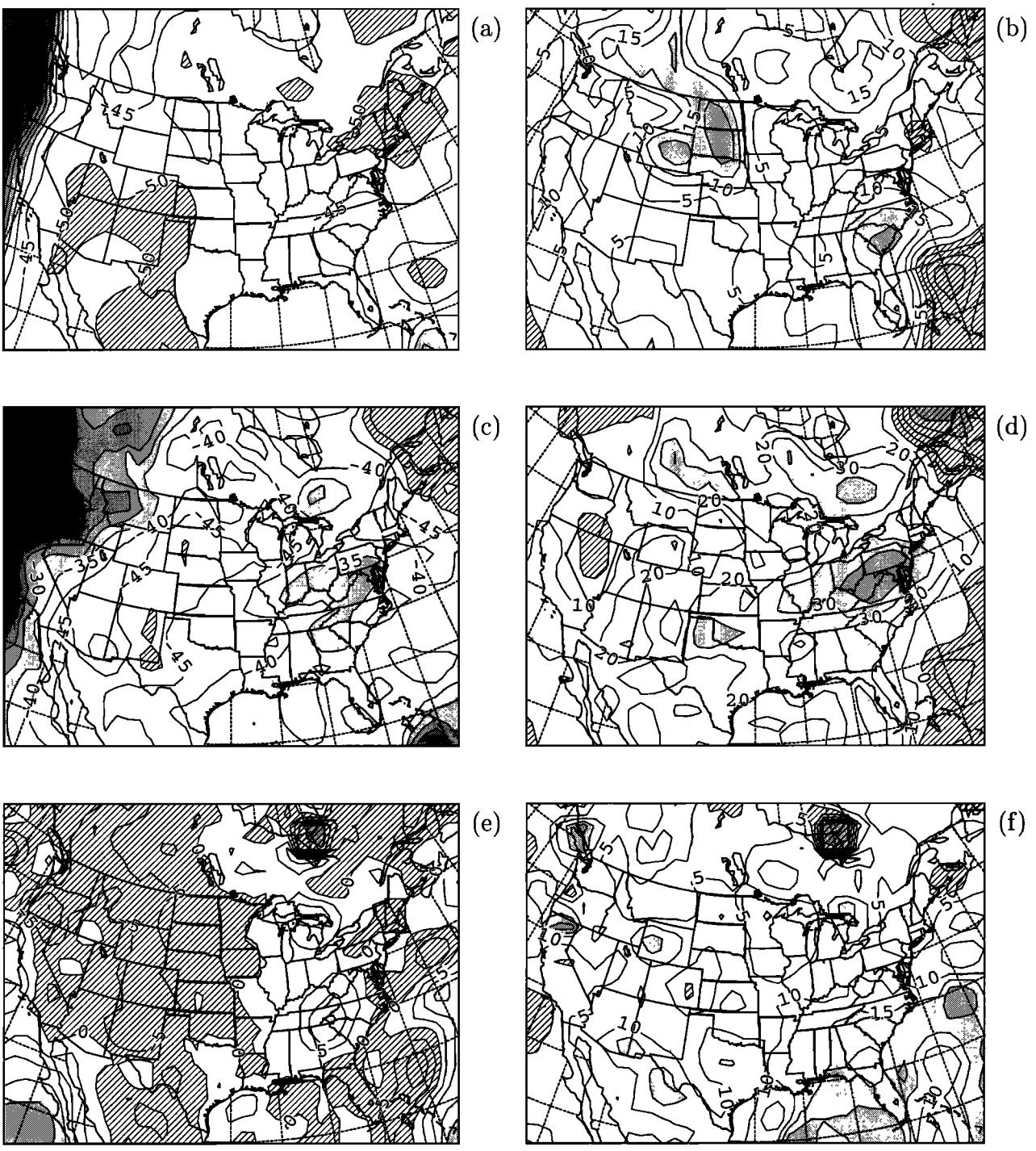

Figure 12. The same as Figure 11 for aerosol during the time period December 6 to 19, 1994. In contrast to Figure 11, a 10% interval is used in Figure 12d.

Atlantic and over Canada in the simulation. Nonlinear responses of the wet deposition are also caused by changes in critical aerosol diameter between the simulations.

The increases in mass mean diameter in some regions over eastern North America (Figure 12e) are explained by the still relatively efficient in-cloud production of SO_4^{2-}, which decreases only by about 30% in these regions. Compared to the simulation at higher SO_2 emissions, the aerosol particles are larger because there are about 50% fewer particles but only a small reduction in in-cloud production of SO_4^{2-}.

A 100% increase in H_2O_2 background concentrations clearly affects the SO_4^{2-} concentrations (Figure 12b), SO_4^{2-} wet deposition (Figure 12d), and SO_4^{2-} mass mean diameter (Figure 12f). The increases are caused

by higher in-cloud production of SO_4^{2-} over most of North America. The increases in in-cloud production of SO_4^{2-} are of the order of 60 to 70% in the most productive regions in eastern North America. The associated changes in SO_4^{2-} concentrations are relatively small owing to low total in-cloud production over the southeastern United States and efficient in-cloud scavenging of SO_4^{2-}. Over the ocean, lower concentrations and wet deposition rates are due to the relatively low importance of in-cloud production involving H_2O_2 and due to reductions in SO_2 concentrations caused by the higher in-cloud oxidation rates over land.

Contrary to the summer period, the results for the responses of SO_4^{2-} wet deposition to SO_x emissions and H_2O_2 background concentrations give evidence that limitations of SO_4^{2-} production in clouds by insufficient H_2O_2 concentrations are of similar importance to SO_2 concentration limitations. Limitations of the SO_4^{2-} in-cloud production due to SO_2 are considerable in the simulation results, especially over more remote regions such as the Rocky Mountains, Canada, and the ocean.

5. Response of CCN Number Concentrations

Since the optical properties and therefore climate effects of clouds are linked to CCN number concentrations, an important question is how CCN number concentrations respond to changes in emissions and atmospheric chemistry. In particular, the relationship between sulphate aerosol concentrations and CCN number concentrations appears to be a source of high uncertainty in the understanding of climate forcing by aerosols [*Hegg*, 1994; *Houghton et al.*, 1996].

To assess the responses of CCN number concentrations to changing SO_x emissions and H_2O_2 background concentrations, only the contribution of sulphate aerosol to the CCN number concentrations is considered in this study. For the July and December periods in 1994, the cumulative CCN number concentration was calculated from integration of the dry sulphate size distribution as function of the critical diameter D_p^{crit}. The mean results at 850 hPa within in the model domain are shown in Figure 13 for three total particle number concentration categories. In the July period, 28% of the values fall into the category $N < 2500$ cm^{-3}, 48% into the category 2500 cm^{-3} $\leq N \leq$ 4500 cm^{-3}, and 24% into the category $N > 4500$ cm^{-3}. For December the respective values are 60%, 18%, and 22%. From these values and the shapes of the cumulative CCN number concentrations it is apparent that the CCN number concentrations in December are lower almost throughout the entire size range from $D_p^{\text{crit}} = 0.01$ μm to $D_p^{\text{crit}} = 1$ μm (Figures 13a and 13b).

A decrease in SO_x emissions by 50% clearly decreases the cumulative CCN number concentrations in the July and December periods (Figures 13c and 13d). It appears that the decreases can be higher or lower than 50%, depending on the values of the critical diameter and the total particle number concentration. Since the results at $N < 2500$ cm^{-3} are less influenced by anthropogenic SO_x emissions than the results at $N \geq 2500$ cm^{-3}, the relative changes in the cumulative CCN number concentrations tend to be smaller compared to the results at higher total particle number concentrations. At $N > 2500$ cm^{-3}, the largest decreases in July are slightly greater than 50% at critical diameters larger than about 0.06 μm. Therefore changes in CCN number concentrations are similar to or slightly larger than changes in SO_x emissions, although decreases in the total aerosol number concentrations are less than 30 to 40% (section 4.1). In December, changes in the cumulative CCN number concentrations are also of the order of 50%. The smallest decrease at about 0.08 μm can be explained by the fact that the mass mean diameter of the aerosol increases in some regions over eastern North America mainly due to only modest decreases in in-cloud SO_4^{2-} production rates but an almost linear decrease in total aerosol number concentration (section 4.2). Accordingly, a high correlation of the changes in cumulative CCN number concentrations at $D_p^{\text{crit}} = 0.08$ μm and the changes in mass mean diameters was obtained in a more detailed comparison of the three-dimensional results (not shown).

A 100% increase in H_2O_2 background concentrations produces similar results for the July and the December periods (Figures 13e and 13f). Whereas the cumulative CCN number concentrations at the smallest critical diameters are almost unchanged compared to the results of the reference simulation, increases occur for critical diameters larger than about 0.07 μm, especially in the December period. These results correspond to the simulated increases in mass mean diameter due to increased in-cloud oxidation of SO_2 at increased H_2O_2 background concentrations during these time periods (sections 4.1 and 4.2). The larger the critical diameter (i.e., the lower the supersaturation) in a cloud, the stronger are the increases in CCN number concentration. However, the increases in the simulations at increased H_2O_2 background concentrations are less than about 10% at CCN number concentrations more than 10 cm^{-3}. Therefore the changes are only relatively small in most of the clouds.

It should also be noted that the above discussion depends on the maximum number of cloud droplets in the simulation, which corresponds to a minimum critical diameter. Since NARCM uses the parameterization of *Martin et al.* [1994], higher cloud droplet number concentration than 375 cm^{-3} cannot occur. This means that aerosol particles with sizes smaller than the corresponding minimum critical diameter are not directly affected by changes in SO_2 in-cloud oxidation rates or scavenging by rain. The maximum concentration of 375 cm^{-3} results from observations of CDNC in marine stratocumulus clouds over the eastern Pacific, South Atlantic, subtropical regions of the North Atlantic, and

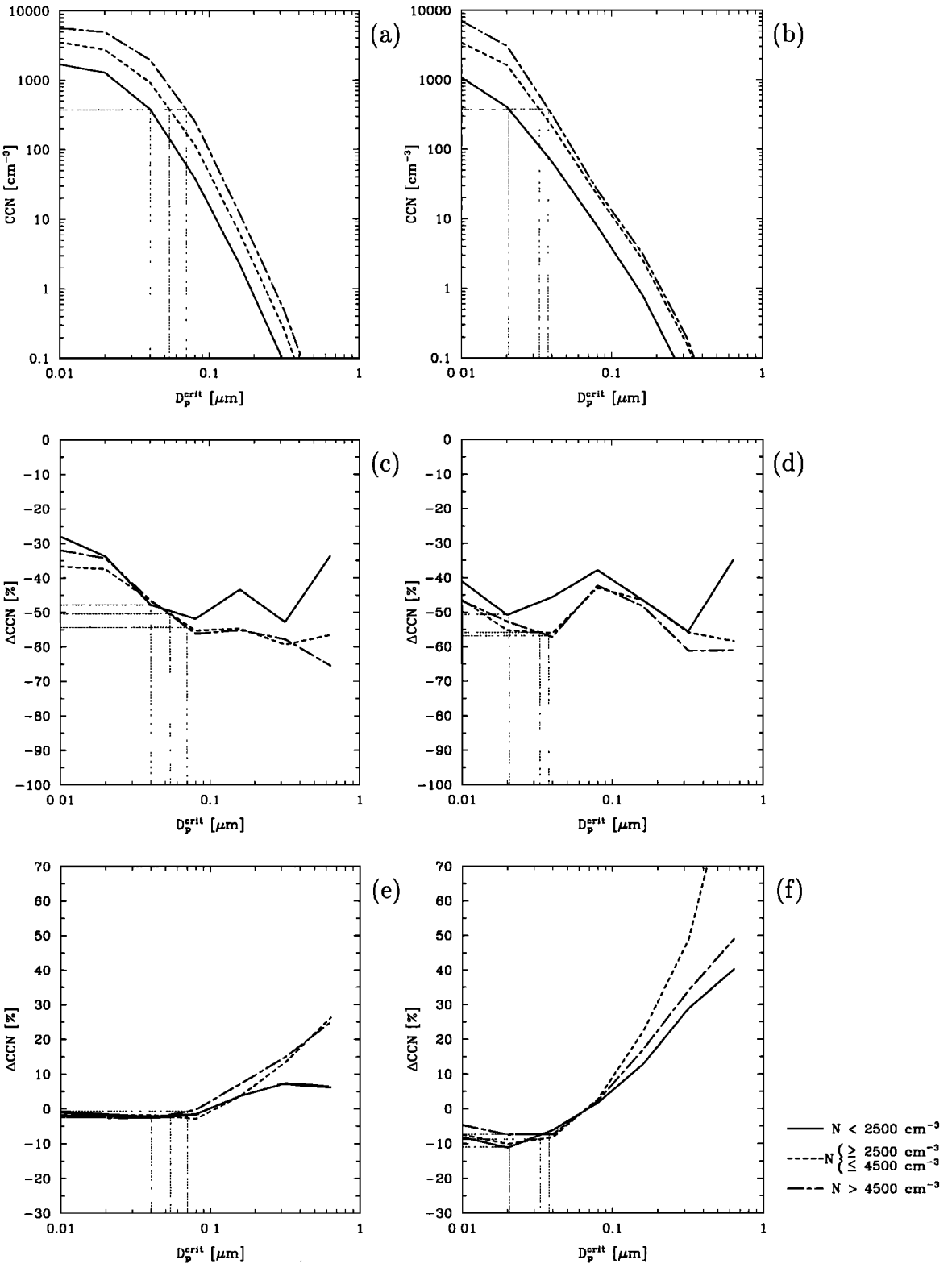

Figure 13. Cumulative CCN number concentration and changes due to 50% reduction in SO_x emissions and 100% increase in H_2O_2 background concentration. Results are shown for the July period in the left column and for the December period in the right column. (a) and (b) Cumulative CCN number concentrations, (c) and (d) changes due to reduced SO_x emissions, and (e) and (f) relative changes due to increased H_2O_2 concentrations. Three categories for the total aerosol number concentration are displayed in each graph. Also shown are the minimum critical diameters in the model in each graph (dotted lines).

the sea areas around the British Isles. The value is certainly too low for deep convective continental clouds which are very important in the present simulations. It can be expected that a more realistic parameterization of aerosol activation would shift the increases in CCN number concentrations shown in Figures 13e and 13f to considerably smaller diameters in the simulations. On the other hand, observations of cloud droplet number concentrations and CCN concentrations at Mount Mitchell in North Carolina in the southeastern United States by *Menon and Saxena* [1998] seem to be in good agreement with the parameterization used in NARCM.

6. Conclusions

Results of simulations of sulphate aerosol size distributions over North America performed for 2-week periods in July and December 1994 have been presented. The simulated mass mean diameter of the sulphate aerosol showed clear regional variations. High values correspond to regions with efficient aerosol growth by in-cloud oxidation and condensation of H_2SO_4. The highest values occur over the major source regions in eastern North America whereas considerably lower values occur over the more remote regions in the west. The sulphate mass mean diameter also depends strongly on relative humidity, clouds, and the occurance of seasalt aerosol in the coastal regions within the model domain. Differences between the simulated mass mean diameters in July and December are mainly caused by changes in relative humidity and cloud amounts.

Comparisons of the results for the July and December periods with observations showed that the mean sulphate concentrations are slightly underpredicted in July and more significantly in December. At least part of the discrepancies can be attributed to differences in relative humidity and precipitation fields between model results and observations. Observed mass mean diameters in three field experiments are about 10 to 20% larger than the corresponding simulated values. This is likely due to the omission of aerosol species other than sulphate and seasalt in the simulation.

The simulation results for July and December were used in sensitivity studies to assess the responses of sulphate aerosol size distributions to artificial decreases in anthropogenic SO_x emissions by 50% and to increases in H_2O_2 background concentrations by 100%. The results give evidence for limitations of in-cloud production due to low abundances of in-cloud SO_2 concentrations in both time periods. In December, limitations due to insufficient H_2O_2 concentrations are also important, especially over the major source regions in eastern North America. Owing to the relatively low cloud amounts over the source regions in eastern North America in both simulations, the clear-sky formation of SO_4^{2-} is of higher importance than the in-cloud formation of SO_4^{2-} in many regions. Mainly as results of SO_2 limitations and the low importance of the in-cloud production of SO_4^{2-}, the SO_4^{2-} concentrations respond approximately linearly to changes in SO_x emissions, and the responses to changes in H_2O_2 background concentrations are relatively small.

The mass mean diameters respond clearly to changes in SO_x emissions and H_2O_2 background concentrations. In response to reduced SO_x emissions, the mass mean diameters decrease by about 10% in July over eastern North America. In the same region, increases in H_2O_2 background concentrations lead to increases in mass mean diameters of up to about 15% in December. Whereas increases in mass mean diameters at higher H_2O_2 background concentrations are explained by more efficient growth of aerosol by higher in-cloud production of SO_4^{2-}, decreases of aerosol sizes at lower SO_x emissions in July are less obvious. The simulation results showed that the aerosol number concentrations decrease by less than 50% due to reductions in SO_x emissions. Since the sulphate concentrations decrease by about 50% at the same time, the mass per aerosol particle is correspondingly reduced.

Reductions in SO_x emissions by 50% result in decreases in CCN number concentrations of between about 30% and 60% for the July period, depending on the critical diameter. The results for the December period are similar. Owing to the significant variations of the CCN number concentrations with critical diameter, it appears that previously suggested relationships between sulphate mass and CCN number concentrations [*Hegg*, 1994; *Boucher and Lohmann*, 1995] are probably too simple to fully describe changes in CCN number concentrations due to changes in SO_x emissions or aerosol number concentrations.

In contrast to the effects of changing SO_x emissions, large increases in CCN number concentrations are simulated at increased H_2O_2 background concentrations and very large critical diameters (compared to threshold values which are assumed in the parameterization of aerosol activation in NARCM). However, the increases are less than about 10% for most of the clouds in the simulations. There is evidence that these increases are underpredicted in the current model version of NARCM. The increases are also expected to be larger on a global scale and under different meteorological conditions due to the relatively low in-cloud SO_4^{2-} production rates in the present simulations.

The results for the CCN number concentrations lead to the hypothesis that increased in-cloud oxidation at high supersaturation (e.g., in convective clouds) due to increases in oxidant concentrations may produce larger CCN which eventually can be easily activated at lower supersaturation (e.g., in stratiform clouds). Such a linkage between oxidant concentrations and CCN concentrations may lead to an additional cooling of the atmosphere in the future since the global concentrations of O_3 and H_2O_2 are predicted to continue to rise [*Thompson et al.*, 1989]. On the other hand, our results also suggest that continuing decreases in SO_x emissions for

North America can be expected to lead to regional decreases in CCN number concentrations in the future. Current and future trends of CCN number concentrations clearly depend on a large variety of processes and emission trends.

Although the simulation results give evidence of a considerable sensitivity of sulphate aerosol size distributions and CCN number concentrations to changes in SO_x emissions and H_2O_2 background concentrations, additional studies have to be performed with an improved version of NARCM to assess the importance of these effects in climate change scenarios. To produce more realistic aerosol size distributions, NARCM will be extended in the future to include organic aerosols and an explicit parameterization of aerosol activation. Other planned model improvements concern the treatment of oxidant chemistry. The photochemical production of H_2O_2 and O_3 will be explicitly included in a future model version in order to improve the effects of meteorology, aqueous phase chemistry, and emissions on oxidant concentrations.

Appendix A: Gas/Droplet Equilibrium

The effective rate constants F_1 and F_2 in (1) are given by

$$F_1 = R_{O_3} f_1 , \quad (A1)$$

$$F_2 = R_{H_2O_2} f_2 . \quad (A2)$$

The rate constants R_{O_3} and $R_{H_2O_2}$ are calculated according to expressions given by *Maahs* [1983] for O_3 and *Martin* [1984] for H_2O_2:

$$R_{O_3} = \{4.4 \times 10^{11} \exp(-4131/T) + 2.6 \times 10^3 \exp(-966/T)\,[H^+]^{-1}\}\ (M\,s)^{-1} ,$$

$$R_{H_2O_2} = 8 \times 10^4 \exp[-3650(1/T - 1/298)]\ \{0.1 + [H^+]\}^{-1}\ (M\,s)^{-1} .$$

In (A1) and (A2) the factors f_1 and f_2 account for the partition of the the species between the aqueous and gaseous phase and depend on the Henry's law coefficients [*Tremblay and Leighton,* 1986; *Leighton et al.,* 1990] of the species:

$$f_1 = \gamma f_{SO_2} f_{O_3} K_S \overline{K}_{HO} , \quad (A3)$$

$$f_2 = \gamma f_{SO_2} f_{H_2O_2} \overline{K}_{HS} \overline{K}_{HP} , \quad (A4)$$

where γ is the dimensionless volume fraction of cloud liquid water. The parameters f_{SO_2}, f_{O_3}, and $f_{H_2O_2}$ are the fractions of the individual species in the gas phase. They are calculated as functions of the dimensionless Henry's law constants $\overline{K}_{HS}$, $\overline{K}_{HO}$, and $\overline{K}_{HP}$:

$$f_{SO_2} = \left(1 + \gamma \overline{K}_{HS} K_S\right)^{-1} , \quad (A5)$$

$$f_{O_3} = \left(1 + \gamma \overline{K}_{HO}\right)^{-1} , \quad (A6)$$

$$f_{H_2O_2} = \left(1 + \gamma \overline{K}_{HP}\right)^{-1} , \quad (A7)$$

with

$$K_S = \overline{K}_{HS} \left(1 + \frac{K_{1S}}{[H^+]} + \frac{K_{1S} K_{2S}}{[H^+]^2}\right) .$$

The Henry's law constants used in (A3) to (A7) are given in Table A1.

Appendix B: Growth of Sulphate Aerosol Due to in-Cloud Oxidation

The general equation describing the growth of aerosol species can be written for bin i as

$$\frac{\partial C_i}{\partial t} = I_i + A_{i-1/2} - A_{i+1/2} ,$$

where I_i is a parameter for formation of the species in bin i, and $A_{i-1/2}$, $A_{i+1/2}$ are parameters for the mass transfer between adjacent bins due to the growth of the particles or droplets [e.g., *von Salzen and Schlünzen,*

Table A1. Equilibrium Constants Used for the Parameterization of the Cloud Chemistry

Equilibrium Relation	Constant Expression	Equilibrium Constant[a] $K(298)$	a	Unit
$SO_2(g) + H_2O(aq) \leftrightarrow SO_2(aq)$	$K_{HS} = \frac{[SO_2(aq)]}{[SO_2(g)]}$	1.23	3120	$\frac{M}{atm}$
$SO_2(aq) \leftrightarrow H^+ + HSO_3^-$	$K_{1S} = \frac{[H^+]\,[HSO_3^-]}{[SO_2(aq)]}$	1.7×10^{-2}	2090	M
$HSO_3^- \leftrightarrow H^+ + SO_3^{2-}$	$K_{2S} = \frac{[H^+]\,[SO_3^{2-}]}{[HSO_3^-]}$	6.0×10^{-8}	1120	M
$O_3(g) + H_2O(aq) \leftrightarrow O_3(aq)$	$K_{HO} = \frac{[O_3(aq)]}{[O_3(g)]}$	1.15×10^{-2}	2560	$\frac{M}{atm}$
$H_2O_2(g) + H_2O(aq) \leftrightarrow H_2O_2(aq)$	$K_{HP} = \frac{[H_2O_2(aq)]}{[H_2O_2(g)]}$	9.7×10^4	6600	$\frac{M}{atm}$

[a]Values reported by *Chameides* [1984]. Constants $K(298)$ and a are in $K = K(298)\,[a\,(1/T - 1/298)]$.

1999a]. The assumption of a purely volume controlled growth of activated sulphate aerosol due to in-cloud oxidation (section 2.1) gives

$$I_i = \frac{C_i}{C_{SO_4^{2-}}} F C_{S(IV)} ,$$

with the sulphate concentration $C_{SO_4^{2-}} = \sum_i C_i$ in the activated aerosol. Simple representations of $A_{i-1/2}$ and $A_{i+1/2}$ can be obtained by using upstream differences:

$$A_j = \frac{C_{j-1/2}}{\Delta\varphi_{j-1/2}} \frac{d\varphi}{dt} , \text{ with } j = i \pm 1/2 .$$

To calculate $d\varphi/dt$, assume the growth of a single sulphate particle by production of additional sulphate due to in-cloud oxidation. Let $m(0)$ be the mass of the particle before and m be the mass after the addition of mass due by in-cloud oxidation. Since

$$\frac{m}{m(0)} = \frac{D_p^3}{D_p^3(0)} = 10^{3(\varphi-\varphi(0))} ,$$

for all particles, it follows that

$$\varphi = \varphi(0) + \frac{1}{3} \log \left(\frac{C_{SO_4^{2-}}}{C_{SO_4^{2-}}(0)} \right) .$$

Finally, calculating $d\varphi/dt$ at $t = 0$ and using the mass balance of sulphur species gives

$$A_j = \frac{C_{j-1/2}}{C_{SO_4^{2-}}} \frac{F C_{S(IV)}}{3 \Delta\varphi_{j-1/2} \ln 10} , \text{ with } j = i \pm 1/2 .$$

Appendix C: Parameterization of Aerosol Nucleation

The nucleation term k_{nucl} and the exponent S for binary homogeneous nucleation of sulphuric acid and water vapor in (8) are parameterized according to the approach of *Kulmala et al.* [1998]. This approach has been reformulated in order to obtain a simple expression of the form given in (8). It can easily be shown that the original approach can be written in this form with

$$k_{nucl} = \exp(b\,d + c)\,(C_{H_2SO_4,c})^{-a} , \qquad \text{(C1)}$$

and the exponent

$$S = a + 0.0102\,b . \qquad \text{(C2)}$$

The sulphuric acid concentration $C_{H_2SO_4,c}$ needed to produce a nucleation rate of 1 particles $cm^{-3}\,s^{-1}$ in (C1) is given (in molecules cm^{-3}) as

$$C_{H_2SO_4,c} = \exp\left(-14.5125 + 0.1335\,T - 10.5462\,RH + 1958.4\,RH/T\right) ,$$

where T denotes the temperature (in K) and RH is the relative humidity divided by 100%. The parameters a, b, c, and d in (C1) and (C2) are given as

$$\begin{aligned} a &= 25.1289 - 4890.8/T - 8.2295 \cdot 10^{-3}\,T\,RH , \\ b &= 7643.3/T - 7.2165 \cdot 10^{-3}\,T/RH , \\ c &= -1743.3/T , \\ d &= 1.2233 - \frac{0.0154\,RA}{RA + RH} - 0.0415 \ln N_w \\ &\quad + 0.0016\,T , \end{aligned}$$

where RA is the relative acidity divided by 100% and N_w is the water vapor concentration (in molecules cm^{-3}).

Finally, the factor g_c in (8) is used to calculate the number of H_2SO_4 molecules produced per s and cm^3 from the nucleation rate $k_{nucl}\,C^S_{H_2SO_4}$ (which is in $cm^{-3}\,s$). For completely dry aerosol, g_c is given by

$$g_c = \frac{\pi\,\rho_p^{dry}\,(D_p^{dry})^3\,N_A}{6\,M_{H_2SO_4}} .$$

Appendix D: Mass Transfer Between Adjacent Bins

The terms $A^N_{i-1/2}$, $A^N_{i+1/2}$, $A^C_{i-1/2}$, and $A^C_{i+1/2}$ in (11) are calculated using the positive definite advection scheme of *Bott* [1989] which can, for example, be written for $A^C_{i-1/2}$ and $A^C_{i+1/2}$ with $j = i \pm 1/2$ and an arbitrary small constant ε as

$$A^C_j = \frac{\max(I^+_{l,j}, 0)}{\max(I_{l,j}, \max(I^+_{l,j}, 0) + \varepsilon)} . \qquad \text{(D1)}$$

The parameters $I^+_{l,j-1/2}$ and $I_{l,j-1/2}$ in (D1) are given as

$$I^+_{l,j} = \sum_{k=0}^{2} \frac{a_{jk}}{(k+1)\,2^{k+1}} \left[1 - (1 - 2\,c_j)^{k+1}\right] \qquad \text{(D2)}$$

$$I_{l,j} = \sum_{k=0}^{2} \frac{a_{jk}}{(k+1)\,2^{k+1}} \left[(-1)^k + 1\right] , \qquad \text{(D3)}$$

with the Courant number c_j given by

$$c_j = \frac{4 \times 10^6\,D\,D_p\,F(Kn)\,A\,M_{H_2SO_4}\,\Delta\varphi_{j-1/2}}{(D_p^{dry})^3\,\rho_p^{dry}\,N_A \ln 10\,\Delta t} C^{t+\Delta t}_{H_2SO_4} , \qquad \text{(D4)}$$

In (D4), ρ_p^{dry} is the dry particle density, N_A is Avogadro's number, and $M_{H_2SO_4}$ is the molar mass of H_2SO_4.

The coefficients a_{ik} in (D2) and (D3) are calculated from the sulphate concentrations in each bin:

$$\begin{aligned} a_{j0} &= C_{j-1/2} , \\ a_{j1} &= 1/2\,(C_{j+1/2} - C_{j-3/2}) , \\ a_{j1} &= 1/2\,(C_{j+1/2} - 2\,C_{j-1/2} + C_{j-3/2}) . \end{aligned}$$

Acknowledgments. We are grateful to Peter Liu and Chul-Un Ro for providing data from the Clean Air Status and Trends Network (CASTNet) and the Canadian Air and Precipitation Monitoring Network (CAPMoN). Further, we would like to thank Frank Dentener for providing ammonia background concentrations and Norm McFarlane for discussions of the cloud chemistry parameterizations. We also thank two anonymous referees for their helpful comments on the manuscript. The research in this article has been funded by the Canadian Institute for Climate Studies through the NARCM project.

References

Albrecht, B., Aerosols, cloud microphysics, and fractional cloudiness, *Science, 245,* 1227-1230, 1989.

Anklin, M., and R. C. Bales, Recent increases in H_2O_2 concentrations at Summit, Greenland, *J. Geophys. Res., 102,* 19,099-19,104, 1997.

Arakawa, A., and W. H. Schubert, Interaction of a cumulus cloud ensemble with the large-scale environment, part I, *J. Atmos. Sci., 31,* 674-701, 1974.

Bates, T. S., B. K. Lamb, A. Guenther, J. Dignon, and R. E. Stoiber, Sulfur emissions to the atmosphere from natural sources, *J. Atmos. Chem., 14,* 315-337, 1992.

Beheng, K. D., A parameterization of warm cloud microphysical conversion processes, *Atmos. Res., 33,* 193-206, 1994.

Benkovitz, C. M., M. T. Scholtz, J. Pacyna, L. Tarrason, J. Dignon, E. C. Voldner, P. A. Spiro, J. A. Logan, and T. E. Graedel, Global gridded inventories of anthropogenic emissions of sulphur and nitrogen, *J. Geophys. Res., 101,* 29,239-29,253, 1996.

Bigalke, K., A new method for incorporating point sources into Eulerian dispersion models, in *Air Pollution Modeling and its Application IX,* edited by H. van Dop and G. Kallos, pp. 651-660, Plenum, New York, 1992.

Bott, A., A positive definite advection scheme obtained by nonlinear renormalization of the advective fluxes, *Mon. Weather Rev., 177,* 1006-1015, 1989.

Boucher, O., and U. Lohmann, The sulfate-CCN-cloud albedo effect; A sensitivity study with two general circulation models, *Tellus, Ser. B, 47,* 197-220, 1995.

Brasseur, G. P., D. A. Hauglustaine, S. Walters, P. J. Rasch, J.-F. Muller, C. Granier, and X. X. Tie, MOZART, a global chemical transport model for ozone and related chemical tracers, 1; Model description, *J. Geophys. Res., 103,* 28,265-28,289, 1998.

Briggs, G. A., Comparison of the trajectories of rising plumes with theoretical empirical models, *Atmos. Environ., 9,* 455-462, 1975.

Caya, D., and R. Laprise, Semi-implicit semi-Lagrangian regional climate model: The Canadian RCM, *Mon. Weather Rev., 127,* 341-362, 1999.

Caya, D., R. Laprise, M. Giguere, G. Bergeron, J.-P. Blanchet, B. J. Stocks, G. J. Boer, and N. A. McFarlane, Description of the Canadian Regional Climate Model, *Water Air Soil Pollut., 82,* 477-482, 1995.

Chameides, W. L., The photochemistry of a remote marine stratiform cloud, *J. Geophys. Res., 89,* 4739-4756, 1984.

Charlson, R. J., S. E. Schwartz, J. M. Hales, R. D. Cess, J. A. Coakley, J. E. Hansen, and D. J. Hoffmann, Climate forcing by anthropogenic aerosols, *Science, 255,* 422-430, 1992.

Choularton, T. W., K. N. Bower, K. M. Beswick, M. Parkin, and A. Kaye, A study on the effects of cloud processing of aerosol on the microphysics of cloud, *Q. J. R. Meteorol. Soc., 124,* 1377-1389, 1998.

Clark, P. A., B. E. A. Fisher, and R. A. Scriven, The wet deposition of sulphate and its relationship to sulphur dioxide emissions, *Atmos. Environ., 21,* 1125-1131, 1987.

Collett, J. L., A. Bator, X. Rao, and B. B. Demoz, Acidity variations across the cloud drop size spectrum and their influence on rates of atmospheric sulfate production, *Geophys. Res. Lett., 21,* 2393-2396, 1994.

DeMore, W. B., S. P. Sander, D. M. Golden, R. F. Hampson, M. J. Kurylo, C. J. Howard, A. R. Ravishankara, C. E. Kolb, and M. J. Molina, Chemical kinetics and photochemical data for use in stratospheric modeling, *JPL Publ., 92-20,* 1992.

Dennis, R. L., J. N. McHenry, S. K. Seilkop, and J. S. Chang, Characterization of the nonlinear change in annual sulfur deposition for a change in emissions, in *Air Pollution Modeling and Its Application VIII,* edited by H. van Dop and D. G. Steyn, pp. 135-143, Plenum, New York, 1991.

Dentener, F. J., and P. J. Crutzen, A three-dimensional model of the global ammonia cycle, *J. Atmos. Chem., 19,* 331-369, 1994.

Eldred, R. A. and T. A. Cahill, Trends in elemental concentrations of fine particles at remote sites in the United States of America, *Atmos. Environ., 28,* 1009-1019, 1994.

Feichter, J., E. Kjellström, H. Rodhe, F. Dentener, J. Lelieveld, and G.-J. Roelofs, Simulation of the tropospheric sulfur cycle in a global climate model, *Atmos. Environ., 30,* 1693-1707, 1996.

Foell, W. K., et al., Energy use, emissions, and air pollution reduction strategies in Asia, *Water Air Soil Pollut., 85,* 2277-2282, 1995.

Gong, S. L., L. A. Barrie, and J.-P. Blanchet, Modeling sea-salt aerosols in the atmosphere, 1; Model development, *J. Geophys. Res., 102,* 3805-3818, 1997a.

Gong, S. L., L. A. Barrie, J. M. Prospero, D. L. Savoie, G. P. Ayers, J.-P. Blanchet, and L. Spacek, Modeling sea-salt aerosols in the atmosphere, 2; Atmospheric concentrations and fluxes, *J. Geophys. Res., 102,* 3819-3830, 1997b.

Graedel, T. E., C. M. Benkovitz, W. C. Keene, D. S. Lee, and G. Marland, Global emissions inventories of acid-related compounds, *Water Air Soil Pollut., 85,* 25-36, 1995.

Gurciullo, C. S., and S. N. Pandis, Effect of composition variations in cloud droplet populations on aqueous-phase chemistry, *J. Geophys. Res., 102,* 9375-9385, 1997.

Hauglustaine, D. A., G. P. Brasseur, S. Walters, P. J. Rasch, J.-F. Muller, L. K. Emmons, and M. A. Carroll, MOZART, a global chemical transport model for ozone and related chemical tracers, 2; Model results and evaluation, *J. Geophys. Res., 103,* 28,291-28,335, 1998.

Hegg, D. A., Cloud condensation nucleus-sulfate mass relationship and cloud albedo, *J. Geophys. Res., 99,* 25,903-25,907, 1994.

Hertel, O., R. Berkowicz, J. Christensen, and O. Hov, Test of two numerical schemes for use in atmospheric transport-chemistry models, *Atmos. Environ., 27,* 2591-2611, 1993.

Holland, D. M., P. P. Principe, and J. E. Sickles, Trends in atmospheric sulfur and nitrogen species in the eastern United States for 1989-1995, *Atmos. Environ., 33,* 37-49, 1999.

Houghton, J. T., B. A. Callander, and S. K. Varney (Eds.), *Climate change 1992: The IPCC Supplementary Report to the IPCC Scientific Assessment, Intergovernmental Panel on Climate Change,* 200 pp., Cambridge Univ. Press, New York, 1992.

Houghton, J. T., L. G. M. Filho, B. A. Callander, N. Narris, A. Kattenberg, and K. Maskell (Eds.), *Climate Change 1995: The Science of Climate Change, Intergovernmental Panel on Climate Change,* 572 pp., Cambridge Univ. Press, New York, 1996.

Hubler, G., et al., An overview of the airborne activities during the Southern Oxidants Study (SOS) 1995 Nashville/Middle Tennessee Ozone Study, *J. Geophys. Res., 103,* 22,245-22,259, 1998.

Kalnay, E. et al., The NCEP/NCAR 40-year reanalysis project, *Bull. Am. Meteorol. Soc., 77,* 437-471, 1996.

Karamchandani, P., and L. K. Peters, Analysis of the error associated with grid representation of point sources, *Atmos. Environ., 82,* 927-933, 1983.

Kasibhatla, P. S., and L. K. Peters, Numerical simulation of transport from a point source: Error analysis, *Atmos. Environ., 24,* 693-702, 1990.

Kettle, A. J., et al., A global database of sea surface dimethylsulfide (DMS) measurements and a procedure to predict sea surface DMS as a function of latitude, longitude, and month, *Global Biochem. Cycles, 13,* 399-444, 1999.

Kleinman, L. I., and P. H. Daum, Vertical distribution of aerosol particles, water vapor, and insoluble trace gases in convectively mixed air, *J. Geophys. Res., 96,* 991-1005, 1991a.

Kleinman, L. I., and P. H. Daum, Oxidant limitation to the formation of H_2SO_4 near a SO_2 source region, *Atmos. Environ., 25,*, 2023-2028, 1991b.

Kleinman, L. I., P. H. Daum, D. G. Imre, J. H. Lee, Y.-N. Lee, L. J. Nunnermacker, S. R. Springston, J. Weinstein-Lloyd, and L. Newman, Ozone production in the New York City urban plume, *J. Geophys. Res.*, in press, 2000.

Kulmala, M., A. Laaksonen, and L. Pirjola, Parameterizations for sulfuric acid/water nucleation rates, *J. Geophys. Res., 103,* 8301-8307, 1998.

Laj, P., et al., Experimental evidence for in-cloud production of aerosol sulphate, *Atmos. Environ., 31,* 2503-2514, 1997.

Laprise, R., D. Caya, G. Bergeron, and M. Giguere, The formulation of Andre Robert MC2 (Mesoscale Compressible Community) model, *Atmos. Ocean, 35,* 195-220, 1997.

Leighton, H. G., M. K. Yau, A. M. Macdonald, J. S. Pitre, and A. Giles, A numerical simulation of the chemistry of a rainband, *Atmos. Environ., 24,* 1211-1217, 1990.

Lelieveld, J., and J. Heintzenberg, Sulfate cooling effect on climate through in-cloud oxidation of anthropogenic SO_2, *Science, 258,* 117-120, 1992.

Levkov, L., B. Rockel, H. Kapitza, and E. Raschke, 3d mesoscale numerical studies of cirrus and stratus clouds by their time and space evolution, *Contrib. Atmos. Phys., 65,* 35-58, 1992.

Lohmann, U., and E. Roeckner, Design and performance of a new cloud microphysics scheme developed for the ECHAM general circulation model, *Clim. Dyn., 12,* 557-572, 1996.

Lohmann, U., K. von Salzen, N. McFarlane, H. G. Leighton, and J. Feichter, Tropospheric sulfur cycle in the Canadian general circulation model, *J. Geophys. Res., 104,* 26,833-26,858, 1999.

Lord, S. J., Interaction of a cumulus cloud ensemble with large-scale environment, part III; Semi-prognostic test of the Arakawa-Schubert cumulus parameterization, *J. Atmos. Sci., 39,* 88–103, 1982.

Maahs, H. G., Kinetics and mechanics of the oxidation of S(IV) by ozone in aqueous solution with particular reference to SO_2 conversion in nonurban tropospheric clouds, *J. Geophys. Res., 88,* 10,721-10,732, 1983.

Malm, W. C., J. F. Sisler, D. Huffman, R. A. Eldred, and T. A. Cahill, Spatial and seasonal trends in particle concentration and optical extinction in the United States, *J. Geophys. Res., 99,* 1347-1370, 1994.

Martin, G. M., D. W. Johnson, and A. Spice, The measurement and parameterization of effective radius of droplets in warm stratocumulus cloud, *J. Atmos. Sci., 51,* 1823-1842, 1994.

Martin, L. R., Kinetic studies of sulfite oxidation in aqueous solution, in *SO_2, NO and NO_2 Oxidation Mechanisms: Atmospheric Considerations,* edited by J. G. Calvert, pp. 63-100, Butterworth-Heinemann, Woburn, Boston, Mass., 1984.

McFarlane, N. A., G. J. Boer, J.-P. Blanchet, and M. Lazare, The Canadian Climate Centre second generation circulation model and its equilibrium climate, *J. Clim., 5,* 1013-1044, 1992.

Meagher, J. F., J. Olszyna, and M. Luria, The effect of SO_2 gas phase oxidation on hydroxyl smog chemistry, *Atmos. Environ., 18,* 2095-2104, 1984.

Meagher, J. F., J. Olszyna, and F. P. Weatherford, The availability of H_2O_2 and O_3 for aqueous phase oxidation of SO_2: The question of linearity, *Atmos. Environ., 24,* 1825-1829, 1990.

Menon, S., and V. K. Saxena, Role of sulfates in regional cloud-climate interactions, *Atmos. Res., 47-48,* 299-315, 1998.

Padro, J., H. H. Neumann, and G. D. Hartog, An investigation of the ADOM dry deposition module using summertime O_3 measurements above a deciduous forest, *Atmos. Environ., 25,* 1689-1704, 1991.

Roelofs, G.-J., Drop size dependent sulfate distribution in a growing cloud, *J. Atmos. Chem., 14,* 109-118, 1992.

Roelofs, G.-J., J. Lelieveld, and L. Ganzeveld, Simulation of global sulfate distribution and the influence of effective cloud drop radii with a coupled photochemistry-sulfur cycle model, *Tellus, Ser. B, 50,* 224-242, 1998.

Russell, L. M., S. N. Pandis, and J. H. Seinfeld, Aerosol production and growth in the marine boundary layer, *J. Geophys. Res., 99,* 20,989-21,003, 1994.

Scott, B. C., Predictions of in-cloud conversion rates of SO_2 to SO_4^{2-} based upon a simple chemical and kinematic storm model, *Atmos. Environ., 16,* 1735-1753, 1982.

Seigneur, C., T. W. Tesche, P. M. Roth, and M.-K. Liu, On the treatment of point source emissions in urban air quality modeling, *Atmos. Environ., 17,* 1655-1676, 1983.

Shannon, J. D., Regional analysis of S emission-deposition trends in North America from 1979 through 1988, in *Air Pollution Modeling and Its Application IX,* edited by H. van Dop and G. Kallos, pp. 57-64, Plenum, New York, 1992.

Slingo, J. M., The development and verification of a cloud prediction scheme for the ECMWF model, *Q. J. R. Meteorol. Soc., 113,* 899-927, 1987.

Slinn, W. G. N., Precipitation scavenging, in *Atmospheric Science and Power Production,* edited by D. Randerson, *DOE/TIC-27601,* pp. 466-532, U.S. Dep. of Energy, Washington, D. C., 1984.

Stockwell, W. R., The effect of gas-phase chemistry on aqueous-phase sulfur dioxide oxidation rates, *J. Atmos. Chem., 19,* 317-329, 1994.

Stockwell, W. R. and J. G. Calvert, The mechanism of HO-SO_2 reaction, *Atmos. Environ., 17,* 2231-2235, 1983.

Tang, I. N., Thermodynamic and optical properties of mixed-salt aerosols of atmospheric importance, *J. Geophys. Res., 102,* 1883-1893, 1997.

Thompson, A. M., M. A. Owens, and R. W. Stewart, Sensitivity of tropospheric hydrogen peroxide to global chemistry and climate change, *Geophys. Res. Lett., 16,* 53-56, 1989.

Tremblay, A., and H. G. Leighton, A three-dimensional cloud chemistry model, *J. Clim. Appl. Meteorol., 25,* 652-671, 1986.

Verseghy, D. L., N. A. McFarlane, and M. Lazare, CLASS - A Canadian land surface scheme for GCMs, II; Vegetation

model and coupled runs, *Int. J. Climatol., 13,* 347-370, 1993.

von Salzen, K., and K. H. Schlünzen, A prognostic physicochemical model of secondary and marine inorganic multicomponent aerosols, I; Model description, *Atmos. Environ., 33,* 567-576, 1999a.

von Salzen, K., and K. H. Schlünzen, A prognostic physicochemical model of secondary and marine inorganic multicomponent aerosols, II; Model tests, *Atmos. Environ., 33,* 1543-1552, 1999b.

Xu, K.-M., and S. K. Krueger, Evaluation of cloudiness parameterizations using a cumulus ensemble model, *Mon. Weather Rev., 119,* 342-367, 1991.

Zhang, G. J., and N. A. McFarlane, Sensitivity of climate simulations to the parameterization of cumulus convection in the Canadian Climate Centre General Circulation Model, *Atmos. Ocean, 33,* 407-446, 1995.

P. A. Ariya and H. G. Leighton, Department of Atmospheric and Oceanic Sciences, McGill University, 805 Sherbrooke Street West, Montreal, Quebec, Canada H3A 2K6. (ariya@omc.lan.mcgill.ca; henry@zephyr.meteo.mcgill.ca)

L. A. Barrie, Atmospheric Sciences and Global Change Resources and Environmental Molecular Science Laboratory, Pacific Northwest National Laboratory, 902 Batelle Boulevard, P.O. Box 999, Richland, Washington 99352. (leonard.barrie@pnl.gov)

J.-P. Blanchet and L. Spacek, Earth Sciences Department, University of Quebec at Montreal, 201 President Kennedy Avenue, Montreal, Quebec, Canada H3C 3P8. (blanchet.jean-pierre@uqam.ca; spacek@atlas.sca.uqam.ca)

S. L. Gong, Meteorological Service of Canada, 4905 Dufferin Street, Toronto, Ontario, Canada M3H 5T4. (sunling.gong@ec.gc.ca)

L. I. Kleinman, Environmental Chemistry Division, Brookhaven National Laboratory, P.O. Box 5000, Upton, New York 11973-5000. (kleinman@bnl.gov)

U. Lohmann, Department of Physics, Dalhousie University, Halifax, Nova Scotia, Canada B3H 3J5. (ulrike@fizz.phys.dal.ca)

K. von Salzen, Canadian Centre for Climate Modelling and Analysis, University of Victoria, P.O. Box 1700, STN CSC, Victoria, British Columbia, Canada V8W 2Y2. (knut.vonsalzen@ec.gc.ca)

(Received September 13, 1999; revised December 1, 1999; accepted January 12, 2000.)